UNIVERSITÀ DEGLI STUDI DI NAPOLI

FEDERICO II

SCUOLA DI DOTTORATO IN

INGEGNERIA INFORMATICA ED AUTOMATICA

DIPARTIMENTO DI INFORMATICA E SISTEMISTICA

MODELING AND CONTROL OF FLEXIBLE STRUCTURES WITH WEAKNESSES

Alessandro Coppola

alessandro.coppola@unina.it

In Partial Fulfillment of the Requirements for the Degree of

PHILOSOPHIAE DOCTOR in

Computer Science and Automation Engineering

November 2010

Tutor	**Coordinator**
Prof. Giovanni Celentano	*Prof. Francesco Garofalo*

UNIVERSITÀ DEGLI STUDI DI NAPOLI

FEDERICO II

SCUOLA DI DOTTORATO IN

INGEGNERIA INFORMATICA ED AUTOMATICA

Date: November 2010

Author: Alessandro Coppola

Title: Modeling and Control of Flexible Structures with Weaknesses

Department: DIPARTIMENTO DI INFORMATICA E SISTEMISTICA

Degree: PHILOSOPHIAE DOCTOR

... to my parents, to my sister and to true colors I see in your eyes…

***Xerxes**:*
"There will be no glory in your sacrifice. I will erase even the memory of Sparta from the histories. The world will never know you existed at all."

***King Leonidas**:*
"The world will know that free men stood against a tyrant, that few stood against many, and before this battle was over, that even a god king can bleed."

AKNOWLEDGEMENT

I deeply thank my advisor Prof. G. Celentano for his valuable and expert advice and Dr. L. Celentano, whose scrupulousness and advices helped me in the development of my researches.

CONTENTS

List of figure……8
List of tables……11
Chapter I - Introduction 13
I.1 Problem statement 13
I.2 Contributions 15
I.2.1 Modeling 15
I.2.2 Trajectory planning and “kinematic” inversion 16
I.2.3 Control 16
I.3 Literature review 17
I.3.4 Flexible robots modeling 17
I.3.5 Flexible robots control 18
Chapter II - A wavelet functions based 20
II.1 Introduction 20
II.2 II. Hypotheses, notations and preliminaries 21
II.3 Lagrangian function of a flexible link 25
II.4 Interconnection algorithm 34
II.5 Dynamic model of the robot 38
II.6 Validation guidelines 39
II.7 A methodology to introduce the internal friction 42
II.8 Properties of the methodology and illustrative examples 43

II.8.1 Static and dynamic precision 43
II.8.2 Numerical stability 54
II.8.3 Computational efficiency 62
Chapter III - A very efficient variation to the assumed mode method 68
III.1 Introduction 68
III.2 Hypotheses, notations and preliminaries 69
III.3 Lagrangian function of a flexible link 70
III.4 Interconnection algorithm and Lagrangian function of the robot 74
III.5 Dynamic model of the robot 77
III.6 A method to reduce the computational cost 79
III.7 Validation results 80
Chapter IV - Trajectory planning 83
IV.1 Introduction 83
IV.2 Presentation of the methodology 83
IV.3 An example of flexible static model derivation 84
Chapter V - Control 87
V.1 Calculation of an admissible nominal input 87
V.2 Controller design 89
V.3 A numerical example 90
Bibliography 96

LIST OF FIGURES

Fig. 1 Schematic representation of a flexible robot. 22
Fig. 2 Schematic representation of the generic flexible link..... 23
Fig. 3 Forces and torques acting on an element ΔL_i of the link. 25
Fig. 4 Fictitious subdivision of the generic link into sublinks. 28
Fig. 5 The considered constraint and loading schemes. 28
Fig. 6 An example of wavelet functions.. 29
Fig. 7 Structure of the matrices B_{fi} and K_i of the *i*-th link..... 33
Fig. 8 Composition scheme of the matrix *B*. 37
Fig. 9 Control actions and disturbances acting on the robot. 39
Fig. 10 Input-output scheme of the robot. 40
Fig. 11 Static deflection of a hinged link with constant cross-section. 41
Fig. 12 Static deflection of a clamped link with constant cross-section. 42
Fig. 13 System of generalized forces equivalent to the gravity action. 44
Fig. 14 Link subjected to a vertical concentrated force not applied to the tip. 45
Fig. 15 *I*-th flexible link having square hollow constant cross-section..... 46
Fig. 16 *I*-th flexible link having square hollow and piecewise constant cross-section. 48
Fig. 17 Static deflection for an ending torque of 50 Nm. 50
Fig. 18 Static deflection for an ending force of 10 N..... 50
Fig. 19 Static deflection due to the gravity payload..... 51
Fig. 20 Frequency responses ending torque – tip rotation of the robot controlled by a strong PD action, with 2 Lagrangian deformation variables per link. 52

Fig. 21 Frequency responses ending torque – tip rotation of the robot controlled by a strong PD action, with 4 Lagrangian deformation variables per link. 52
Fig. 22 Frequency responses ending torque – tip rotation of the robot controlled by a weak PD action, with with 2 Lagrangian deformation variables per link. 53
Fig. 23 Frequency responses ending torque – tip rotation of the robot controlled by a weak PD action, with with 4 Lagrangian deformation variables per link. 54
Fig. 24 Frequency responses ending torque – tip rotation with 2 Lagrangian deformation variables per link. 55
Fig. 25 Frequency responses ending torque – tip rotation with 10 Lagrangian deformation variables per link. 56
Fig. 26. Single link flexible robot. 57
Fig. 27 *I*-th flexible link having square hollow and linearly varying cross-section. 60
Fig. 28 Frequency responses ending torque – tip rotation with 2 Lagrangian deformation variables per link. 61
Fig. 29 Frequency responses ending torque – tip rotation with 10 Lagrangian deformation variables per link. 62
Fig. 30 Time histories of the terminal deflections δ_i of the three links. 66
Fig. 31 A detail of Fig. 30. 66
Fig. 32 A detail of the time histories of the terminal rotations γ_i of the three links. 67
Fig. 33 Schematic representation of a flexible link. 69
Fig. 34 Composition scheme of the matrix *B*. 76
Fig. 35 Control actions and disturbances acting on the robot. 78
Fig. 36 *I*-th flexible link having square hollow constant cross-section. 81
Fig. 37 Two-link flexible robot. 85

Fig. 38 Simulink block scheme for the calculation of an admissible input. 88
Fig. 39 Flexible robot poses in correspondence of the trajectory points. 91
Fig. 40 The desired joint trajectory obtained through interpolation (joint 1 in blue, joint 2 in green). 92
Fig. 41 Admissible nominal input. 92
Fig. 42 Time diagram of the Lagrangian deformation variable δ_2 (100% of the initial conditions in blue, 90% of the initial conditions in green, 80% of the initial conditions in red)..... 93
Fig. 43 Time diagram of the x and y coordinates of the tip. 94

LIST OF TABLES

Table I First two frequencies of the robot with clamped links having constant cross-section. 47
Table II Tip rotation for concentrated torque and force applied to the tip and for the gravitational payload. 47
Table III Vertical tip displacement for concentrated torque and force applied to the tip and for the gravitational payload. 47
Table IV Tip rotation for ending torque and force and for gravitational payload. 49
Table V Vertical tip displacement for ending torque and force and for gravitational payload. 49
Table VI Condition numbers of the inertia matrices when the number of deformation freedom degrees increases. 54
Table VII Number of multiplications with 4 deformation variables per link. 63
Table VIII Number of multiplications with 8 deformation variables per link. 63
Table IX Time costs of the dynamic simulation with 4 Lagrangian deformation variables per link. 64
Table X Time costs of the dynamic simulation with 6 Lagrangian deformation variables per link. 64
Table XI Time costs of the dynamic simulation with 8 Lagrangian deformation variables per link. 65
Table XII Number of multiplications to evaluate the inertia matrix B with 4 modes per link. 81
Table XIII Number of multiplications to evaluate the gradient of the kinetic energy c with 4 modes per link. 81

Table XIV Number of multiplications to evaluate the inertia matrix B with 3 links. 82
Table XV Number of multiplications to evaluate the gradient of the kinetic energy c with 3 links. 82

CHAPTER I - INTRODUCTION

I.1 Problem statement

The modeling of flexible robots and, more generally, the modeling of flexible structures having weaknesses controlled or not, is a historic topic of robotic research [2] [7]-[14] and it remains very interesting for the scientific community [37], [38], [42], [44], [45].

The derivation of the dynamic model of a robot is fundamental for its dimensioning, for the design of the control system and for its validation making suitable simulations. Several methods have been proposed in literature for these purposes, such as the Newton-Euler method [3] [4], the Kane's method [6] and the Euler-Lagrange one [5], [12]. However, the above methods are useful only when each link of the robot is considered a rigid body.

Many researchers and engineers over the years have realized that flexible robots are lighter, faster, and cheaper than similar rigid robots. These benefits are important in aerospace applications, where structures must be lightweight, but also in the transport and manufacturing systems employed in modern mass production plants.

In fact, the above systems require higher and higher specifications in terms of operating speeds and/or amplitude of the work space; the only way to satisfy the previous specifications is to reduce the mass and to make the structures slender, thus to employ robots having flexibility properties.

Obviously, in order to take full advantage of the benefits offered by the above lightweight flexible robots, it is necessary to develop modeling methodologies which allow to obtain reliable and efficient models and to develop trajectory planning and control methodologies.

The modeling, planning and control of realistic flexible robots represent a research area with significant problems to face, like, for example, the followings:

- the derivation of a model which is precise under the assumption of almost static motion and at low frequencies, since flexible structures must be almost always operated and/or solicited at low frequencies, in order to avoid their breaking and/or annoying noises;
- the choice of mode shape functions and/or of admissible basis functions to describe the flexible behavior;
- the integration of the structure model with the sensors and actuators ones;
- the numerical stability of the models with "small" errors;
- the computational load, since the models of flexible structures, because of their weaknesses, are strongly nonlinear and very complex, even for small deformations;
- the "kinematic" inversion, which is a complex problem because of the structure flexibility and of the external and mass forces, in particular the gravity one;
- the distributed parameter model of the flexible structure makes the control problem hard to solve, since the Lagrangian deformation variables used to approximate the structure flexibility are almost always not directly controllable, i.e. a joint controlled flexible structure is a sub-actuated system;
- the closed loop control system must exhibit robustness properties in order to avoid the troublesome and/or dangerous spillover

This paper presents a methodology which gives significant answers to the above problems, which are extremely relevant especially if the control problem is

considered; some results related to the active control of vibrations of static structures have already been given in [21], [24], and some ideas related to flexible structures with weaknesses have already been presented in [39], [43].

I.2 Contributions

The contributions of this work fall into the areas of modeling, trajectory planning, "kinematic" inversion and control of flexible structures.

I.2.1 Modeling

In this Ph.D thesis a modular, computationally efficient, and numerically stable method is presented, which allows to obtain the dynamic model of a robot constituted by flexible links having variable cross-section and subjected to generic ending forces and torques and to the gravity actions.

This method is based on the use of admissible deformation functions of wavelet type, obtained by using the *Instantaneity Principle of the deflection of an element*, and it is based on the Euler-Bernoulli beam theory if the link is slender or, otherwise, on the Timoshenko one. Moreover, it is easy to extend the presented methodology to deal also with the case of large link deformations.

Moreover, a very simple method to obtain the analytical model of a flexible robot has been developed, which results drastically more efficient, from a computational point of view, than the assumed modes method.

This method uses suitable linear combinations of the modes of each link as basis functions to evaluate the deflection, such a way to minimize the dependency of the position of the generic link on the Lagrangian variables of the previous links.

Finally, a simple and efficient technique to insert friction into the dynamic model of a flexible robot has been developed.

I.2.2 Trajectory planning and "kinematic" inversion

A technique for the trajectories planning has been developed, which consists in defining a certain number of points in the operational space; in each point, a "kinematic" inversion is performed, which is based on the nonlinear static flexible model of the robot; the above model is derived by using the sectioning and congruence techniques known by the building science.

The desired joint trajectory is then obtained through suitable interpolation of the joint variables and by "decoupling the flexible dynamics from the rigid ones".

I.2.3 Control

A method which allows to find, given a desired joint trajectory, an admissible nominal input has been developed; this input is compatible with the whole rigid-flexible dynamics and it allows to obtain the above trajectory.

However, since the nominal model is unstable, it is stabilized in a sufficiently high number of points by using easily implementable controllers, which are designed with the use of a parameter optimization technique.

Then the control law is then calculated by interpolating the gains of the controllers in the various points; in this way, a controller is obtained, whose gains are nonlinear functions of the rigid motion coordinates and, possibly, of some measurable deformation coordinates.

The designed control law is finally validated by verifying the convergence to zero of the impulse response matrix, which is numerically calculated, and/or by using the Lyapunov theory.

I.3 Literature review

The literature review is divided into two areas: the modeling and the control of flexible robots.

I.3.4 Flexible robots modeling

In order to describe the behavior of a flexible robot it is possible to use infinite dimensional models, exact but scarcely operative, or finite dimensional models, which are approximate but more operative.

The most known approximate methods in literature are the assumed modes method, the Ritz-Kantorovich expansions with polynomials, and the finite elements and finite differences methods.

The assumed mode method [8], [9], [14], [16], [28], [32], [41] uses the modes deriving from the solution of the Euler-Bernoulli beam dynamic equation with distributed inertial load and no other loads.

This equation is solved by imposing 4 boundary conditions which describe the configuration of the flexible link. In some works [16] [44], the configuration of the link with clamped-free boundary conditions has been proposed, in other works [9], [14], instead, the one with clamped-mass boundary conditions has been considered.

However, these choices are not appropriate to describe the varying configurations of the flexible link in which occurs when it is joined to other links and/or when it is subjected to gravity actions, disturbances and under joint control actions, also in static conditions. Moreover, the assumed mode method presents other drawbacks: first the derivation of modes becomes very complicated because they can be obtained only in a numerical way, in particular when the link has variable cross-section, secondly the modes are very sensitive to parametric variations.

The Ritz-Kantorovich [10], [20] expansion uses the polynomial set in order to approximate the deflection. This choice results to be inappropriate in the realistic case of links having variable cross-section, even at very low frequencies; moreover, in any case, it produces serious problems of numerical instability, also when the cross-section is constant, when a high precision is needed in a large bandwidth of mechanical solicitations, as it will be shown in the sequel.

The finite elements approach [7], [23], [32] requires the use of cumbersome software packages which are often not control oriented. Also if a specific FEM software can model the structure, this model cannot be easily used to design the control system. Moreover, the modeling of multi-body dynamics and their integration with sensors and actuators models can be burdensome for a control engineer who is not an expert in FEM.

I.3.5 Flexible robots control

Several control techniques exist in literature, many of which have been applied to flexible robots.

The application of pole-placement techniques to flexible systems is discussed in [2]; these techniques are able to move lightly damped poles to locations with higher damping.

In [11] a singular perturbation approach is developed to the control of flexible-link manipulators. This approach consists in breaking the system into two subsystems; the former is slow and describes the rigid motion, the latter is fast and describes the vibrations about the nominal motion of the slow subsystem. Rigid robot control techniques are applied to the slow subsystem, and then a stabilizing controller is developed for the fast subsystem.

In [22] the above work is extended to control the position of a flexible robot as well as its contact force with a rigid environment.

In [13] an approach for designing optimal compensators for the slow and fast subsystems is presented. Care is taken to ensure that fast subsystem spillover does not destabilize the slow subsystem.

In [18] a problem formulation directly based on PDE without discretization is presented; by using the concept of A-dependent operators in Hilbert spaces, a rigorous proof of the ability of direct strain feedback control to damp vibrations for a single-flexible-link robot is given. However, the torque control requires the feedback of strain rate, which is difficult to measure in practice.

In [33] [35] [34] an adaptive control based on neural networks has been applied to several flexible systems. This approach has been shown to be effective in compensating for parametric errors, unmodeled dynamics, external disturbances, and actuator nonlinearities.

Other modeling methodologies which have been applied to flexible robots are the H_∞ robust control [15], [30] and the sliding mode control [30], [26], even if mainly in the case of a single-link flexible robot.

CHAPTER II - A WAVELET FUNCTIONS BASED MODELING METHODOLOGY

II.1 Introduction

In this chapter a modular, computationally efficient, and numerically stable method is presented, which allows to obtain the dynamic model of a robot constituted by flexible links having variable cross-section and subjected to generic ending forces and torques and to the gravity actions. This method is based on the use of admissible deformation functions of wavelet type, obtained by using the *Instantaneity Principle of the deflection of an element*, and it is based on the Euler-Bernoulli beam theory if the link is slender or, otherwise, on the Timoshenko one.

Moreover, it is easy to extend the presented methodology to deal also with the case of large link deformations.

The kinematic model of the generic link is obtained by using absolute motion and relative deformation coordinates; the dynamic model, derived with the Lagrangian approach, is obtained by assembling the Lagrangian functions of the links, which are obtained una tantum in an analytical compact form, by using a very simple recursive interconnection algorithm based on the congruence technique.

The proposed modeling methodology guarantees no static error, even with a relatively low number of wavelet functions per link (in the planar case at least 2), both in the presence of generic forces and torques at both ends, for generic cross-section profiles, and in the presence of gravity actions, for several cross-section ones; moreover, it guarantees good dynamic precision at low frequencies with a contained number of wavelet functions per link and a dynamic precision which increases when the number of wavelet functions increases; this happens in an

increasing frequency range as long as this range and the entity of deformations make the infinite dimensional model of Bernoulli or Timoshenko still valid.
It is shown that the presented methodology is also more efficient and numerically stable than other modeling methods known in literature.
In this chapter some effective methods of static and dynamic comparison, between the proposed methodology to model realistic flexible robots and others very significant in literature, are also proposed and applied.
Moreover, some significant examples are presented in this paper which highlight that the proposed modelling methodology is advisable when it is necessary to obtain high precisions, in particular at low frequencies, and/or not prohibitive calculus time and/or when the other modelling methods result inapplicable because of numerical divergence problems.
This methodology can be used to obtain models for the dynamic simulation of flexible robots and/or for the design of the control system and for the analysis of its performance.
The results presented in this chapter are based on [46], [48].

II.2 II. Hypotheses, notations and preliminaries

In this paper it is considered, for brevity, the case of a planar robot with fixed base, constituted by ν flexible links having variable cross-section. For simplicity, each link has a straight line as unstressed configuration, both rigid ends of negligible dimensions with respect to its length, and rotation axes orthogonal to the vertical plane. It is worth noting that the modeling methodology can be easily extended to more complex robots.

In Fig. 1 a schematic representation of a planar flexible robot with three links is shown, while in Fig. 2 a detailed representation of the i-th link in the stressed and unstressed configuration is reported.

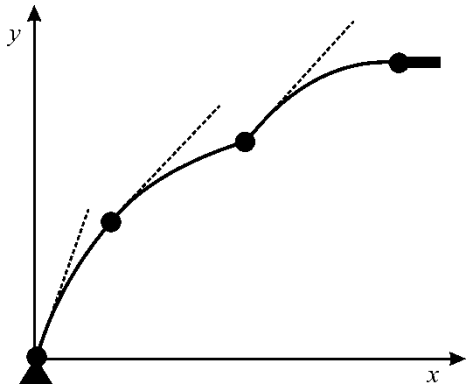

Fig. 1 Schematic representation of a flexible robot.

For the sake of clarity, the following preliminary notations are introduced for the generic *i*-th link:

- L_i is the length of the link;
- A_i is the cross-section area of the link;
- E_i is the modulus of normal elasticity of the link;
- G_i is the modulus of transversal elasticity of the link;
- χ_i is the shear factor of the link;
- I_i is the area moment of inertia for the cross-section of the link;
- ρ_i is the mass density of the flexible part of the link;
- $m_i = \rho_i A_i$ is the mass per unit length of the flexible part of the link;
- M_i^-, M_i^+ are the masses of the rigid ends of the link;

- J_i^-, J_i^+ are the inertia moments of the rigid ends of the link with respect to rotation axes;
- q_i is the distributed transversal load;
- τ_i are the distributed torques;
- x_{oi}, y_{oi}, α_i are the absolute motion coordinates of the link supposed rigid;
- $d_i(z,t)$ is the relative vertical deflection of the link;
- $\gamma_i(z,t)$ is the rotation of the generic cross-section of the link;

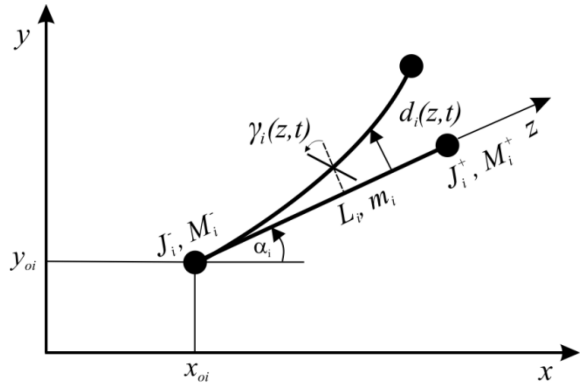

Fig. 2 Schematic representation of the generic flexible link.

Moreover, suppose that the following result holds.

Instantaneity Principle of the deflection of an element. If the inertia of an element ΔL_i of "sufficiently small" length of the *i*-th link is neglected, the vertical deflection of this element, due to "slowly variable" control actions and/or disturbances acting on the links and on the end-effector and due to the consequent inertial actions, remains practically unchanged.

Remark 1. It is worth noting that, according to the sectioning principle of a structure, the deflection of the element is due to (Fig. 3):

- the torque C^- and the force T^- acting on the left end of the element, corresponding to the resultant of all external torques and forces with changed sign, including gravity actions, constraints actions and inertial forces acting on the left-hand side of the robot;
- the torque C^+ and the force T^+ acting on the right end of the element, corresponding to the resultant of all external torques and forces, including gravity actions, constraints actions due to interaction with the environment and inertial forces acting on the right-hand side of the robot with its possible payload;
- the generalized forces acting on the element itself including gravitational actions, disturbances and inertial actions.

Therefore, for the calculus of the deflection of the element, it is possible to neglect the inertial actions acting on the element itself. This approximation is as true as the element is small, as the flexible parts of the links are lightweight with respect to the whole robot, also with actuators, and as the motion is slow.

These remarks justify the Instantaneity Principle.

The Instantaneity Principle and the Euler-Lagrange theory represent the key on which the presented modeling methodology is based.

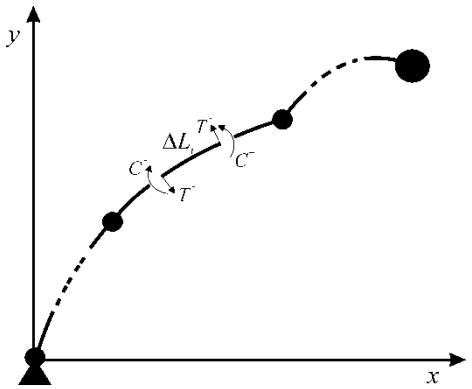

Fig. 3 Forces and torques acting on an element ΔL_i of the link.

II.3 Lagrangian function of a flexible link

In this paragraph the Lagrangian function of a flexible link, supposed in free-free boundary conditions, is derived, in a compact and closed form, by using the Euler-Bernoulli or the Timoshenko [1] beam theories and the Instantaneity Principle of the deflection of an element

According to the preliminary notations (see also Fig. 2), the configuration of the generic cross-section of the *i*-th link can be expressed as:

$$\begin{aligned} x_i &= x_{oi} + z\cos(\alpha_i) - d_i \sin(\alpha_i) \\ y_i &= y_{oi} + z\sin(\alpha_i) + d_i \cos(\alpha_i) \\ \psi_i &= \alpha_i + \gamma_i . \end{aligned} \tag{1}$$

Several methods to approximate the deflection $d_i(z,t)$ of a flexible link have been proposed in literature. These methods consist in choosing a complete set of functions $\{m_k(z)\}$ through which the deflection can be approximated as

$d_i(z,t) \approx \sum_{k=1}^{n} m_k(z) q_{fk}(t)$, where $q_{fk}(t)$ are the Lagrangian deformation variables; moreover, almost always it is supposed that $\gamma_i = \partial d_i / \partial z$.

Different choices of the set $\{m_k(z)\}$ have been proposed in literature. The assumed mode method uses the modes deriving from the solution of the Euler-Bernoulli beam dynamic equation with distributed inertial load and with $q(z,t) = 0$

$$\frac{\partial^2}{\partial z^2}\left(E(z)I(z)\frac{\partial^2 d(z,t)}{\partial z^2} \right) + m(z)\frac{\partial^2 d(z,t)}{\partial t^2} = q(z,t). \tag{2}$$

Equation (2) is solved by imposing 4 boundary conditions which describe the configuration of the flexible link. In some works [16], [44] , the configuration of the link with clamped-free boundary conditions has been proposed, in other works [9], [14], instead, the one with clamped-mass boundary conditions has been considered. However, these choices are not appropriate to describe the varying configurations of the flexible link in which occurs when it is joined to other links and/or when it is subjected to gravity actions, disturbances and under joint control actions, also in static conditions. Moreover, the assumed mode method presents other drawbacks: first the derivation of modes becomes very complicated because they can be obtained only in a numerical way, in particular when the link has variable cross-section, secondly the modes are very sensitive to parameter variations.

In other works [10], [20] the polynomial set $m_k(z) = z^k$ has been chosen as complete set of functions $\{m_k(z)\}$. This choice proves to be inappropriate in the realistic case of links having variable cross-section, even at very low frequencies,

and, in any case, it produces serious problems of numerical instability, also if the cross-section is constant, when a high precision is needed in a large bandwidth of mechanical solicitations. According to the Instantaneity Principle and to Remark the deflection of the generic element of the link is computed with the proposed method by approximating the dynamic beam equation of Euler-Bernoulli (2) with the following static equation

$$\frac{\partial^2}{\partial z^2}\left(E(z)I(z)\frac{\partial^2 d(z,t)}{\partial z^2}\right) = q(z,t)\,, \tag{3}$$

which is obtained by neglecting the inertial term and by considering time-independent loads.

If the shear effect is not negligible, the deflection of the generic element of the link can be computed more accurately by approximating the dynamic beam equations of Timoshenko [1]

$$\begin{aligned} &\frac{\partial}{\partial z}\left(\frac{GA}{\chi}\left(\frac{\partial d}{\partial z} - \gamma \right)\right) - m\frac{\partial^2 d}{\partial t^2} = -q \\ &\frac{\partial}{\partial z}\left(EI\frac{\partial \gamma}{\partial z}\right) + \frac{GA}{\chi}\left(\frac{\partial d}{\partial z} - \gamma \right) - \rho I\frac{\partial^2 \gamma}{\partial t^2} = \tau \end{aligned} \tag{4}$$

in which the dependency on z and t has been omitted, with the static ones. Finally, if the link is subjected to large deformations [25], it is still possible to apply the proposed methodology, by fictitiously subdividing the link into sublinks as shown in Fig. 4.

The above static equations, with suitable boundary and “middle” conditions, with concentrated loads in the middle and/or at the ends, and/or with distributed loads according to the mass density or according to its first order moment, are

numerically or analytically, if it is possible, solved on any interval Z_k of an appropriate partition of the monodimensional domain of the *i*-th link. For example, by assuming that the generic domain $[0, L_i]$ is uniformly partitioned into n_i parts, the intervals Z_k are defined as follows

$$\left\{\left[0, 2\frac{L_i}{n_i}\right], \left[\frac{L_i}{n_i}, 3\frac{L_i}{n_i}\right], \ldots, \left[(n_i - 1)\frac{L_i}{n_i}, L_i\right]\right\}. \tag{5}$$

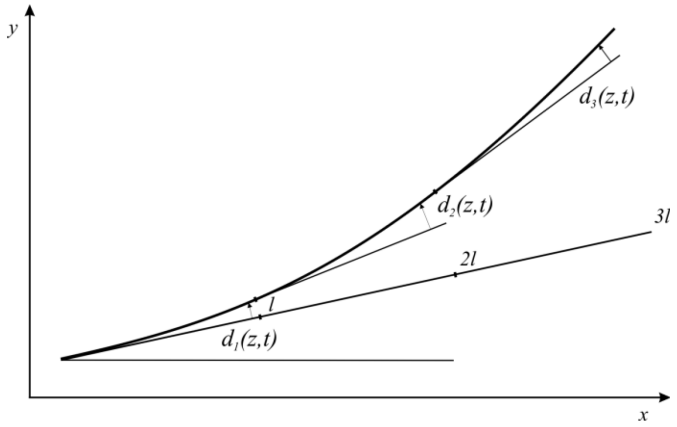

Fig. 4 Fictitious subdivision of the generic link into sublinks.

In Fig. 5 the constraint and the static loading physical schemes of a partition element, considered in the following, are reported.

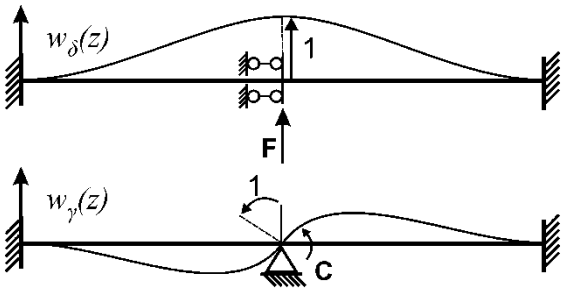

Fig. 5 The considered constraint and loading schemes.

The deflections $w_{\delta k}$, $w_{\gamma k}$ corresponding to the considered schemes, derived for the interval $Z_k = \left[Z_k^-, Z_k^+ \right]$ (k=1,2,…n_i) of the partition, represent the wavelet spatial functions used by the proposed methodology in order to approximate the vertical displacement and the rotation due to the deformation. An example of these wavelet functions, under the hypothesis that $Z_1 = \left[0 \quad 2L_i/3 \right]$, $Z_2 = \left[L_i/3 \quad L_i \right]$ and $Z_3 = \left[2L_i/3 \quad L_i \right]$, is reported in Fig. 6.

Once the wavelet functions have been calculated, the deflection of the i-th link is approximated as

$$d_i(z,t) = \sum_{k=1}^{n_i} \left(w_{\delta k}(z)\delta_k(t) + w_{\gamma k}(z)\gamma_k(t) \right).$$

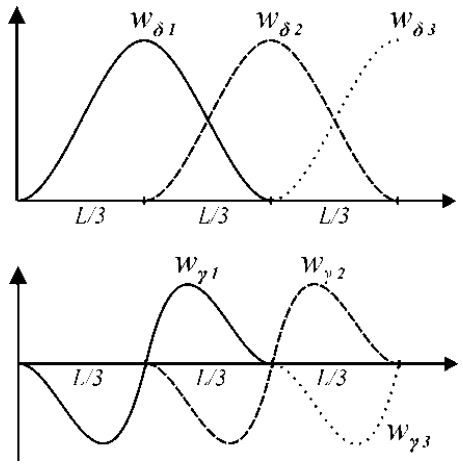

Fig. 6 An example of wavelet functions..

Remark 2. It is worth noting that the Lagrangian deformation variables δ_{ik}, γ_{ik} corresponding to these wavelet functions respectively represent the vertical displacements and the rotations of the cross-sections of the link in correspondence to the endpoints of the partition intervals Z_k.

After these preliminary considerations, by neglecting the contribute of the rotation due to the deformation, the kinetic energy of the *i*-th link can be derived as follows

$$T_i = \frac{1}{2}\int_0^{L_i} (\dot{x}_i^2 + \dot{y}_i^2) m_i(z) dz + \frac{1}{2} M_i^- (\dot{x}_{oi}^2 + \dot{y}_{oi}^2) + \frac{1}{2} J_i^- \dot{\alpha}_i^2 + \frac{1}{2} M_i^+ (\dot{x}_i^2 \Big|_{z=L_i} + \dot{y}_i^2 \Big|_{z=L_i}) + \\ + \frac{1}{2} J_i^+ \left(\dot{\alpha}_i + \dot{\gamma}_{in_i}\right)^2 . \tag{6}$$

After some tedious manipulations and by omitting, for the simplicity of notations, the subscript *i*, it is

$$T = \frac{1}{2}\Big\{ M\left(\dot{x}_o^2 + \dot{y}_o^2\right) + M^+ \dot{\delta}_n^2 + J^+ \dot{\gamma}_n^2 + \left(J + q_f^T B_f q_f + M^+\left(L^2 + \delta_n^2\right)\right)\dot{\alpha}^2 + \dot{q}_f^T B_f \dot{q}_f + \\ + 2\left(k^T \dot{q}_f + J^+ \dot{\gamma}_n + M^+ L \dot{\delta}_n\right)\dot{\alpha} - 2\left(M^+ \delta_n + h^T q_f\right)\dot{\alpha}\left(\dot{x}_o \cos\alpha + \dot{y}_o \sin\alpha\right) + \\ + 2\left(N\dot{\alpha} + h^T \dot{q}_f + M^+ \dot{\delta}_n\right)\left(\dot{y}_o \cos\alpha - \dot{x}_o \sin\alpha\right)\Big\} , \tag{7}$$

where, by omitting the dependency on *z*:

- $M = M^- + \int_0^L m(z) dz + M^+ ,\ J = J^- + \int_0^L z^2 m(z) dz + J^+ ,\ N = M^+ L + \int_o^L z m(z) dz ;$ (8)

- the symmetric matrix $B_f \in R^{2n\times 2n}$ is derived by using the relationship

$$B_f = \begin{bmatrix} \int_0^L w_{\delta 1}^2 m dz & - & - & - \\ \int_0^L w_{\delta 1} w_{\gamma 1} m dz & \int_0^L w_{\gamma 1}^2 m dz & - & - \\ \vdots & \vdots & \ddots & - \\ \int_0^L w_{\delta 1} w_{\gamma n} m dz & \int_0^L w_{\gamma 1} w_{\gamma n} m dz & \cdots & \int_0^L w_{\gamma n}^2 m dz \end{bmatrix} \tag{9}$$

- the vector $h \in R^{2n}$ is derived by using the relationship

$$h^T = \begin{bmatrix} \int_0^L w_{\delta 1}\, m\, dz & \int_0^L w_{\gamma 1}\, m\, dz & \cdots & \int_0^L w_{\gamma n}\, m\, dz \end{bmatrix} \tag{10}$$

- the vector $k \in R^{2n}$ is derived by using the relationship

$$k^T = \begin{bmatrix} \int_0^L w_{\delta 1}\, m\, z\, dz & \int_0^L w_{\gamma 1}\, m\, z\, dz & \cdots & \int_0^L w_{\gamma n}\, m\, z\, dz \end{bmatrix} \tag{11}$$

- $q_f \in R^{2n}$ represents the vector of the Lagrangian deformation coordinates

$$q_f^T = \begin{bmatrix} \delta_1 & \gamma_1 & \cdots & \delta_k & \gamma_k & \cdots & \delta_{n_i} & \gamma_{n_i} \end{bmatrix}, \tag{12}$$

where, according to Remark 2, δ_k and γ_k respectively represent the vertical displacements and the rotations of the cross-sections, due to the deformation, of the link in correspondence to the endpoints of the intervals Z_j of the partition.
Once the kinetic energy has been derived, it is necessary to calculate the elastic potential energy U_{ei} and the gravitational potential one of the *i*-th link.

The elastic potential energy due to the deformation of the *i*-th link, neglecting the contribute due to shear, results

$$U_e = \frac{1}{2}\int_0^L \left(\frac{\partial^2 d}{\partial z^2}\right)^2 E(z)I(z)dz = \frac{1}{2} q_f^T K q_f \ , \tag{13}$$

where the symmetric matrix $K \in R^{2n\times 2n}$ is derived by using the relationship

$$K = \begin{bmatrix} \int_0^L w''_{\delta 1}{}^2 E\,I\,dz & - & - & - \\ \int_0^L w''_{\delta 1} w''_{\gamma 1} E\,I\,dz & \int_0^L w''_{\gamma 1}{}^2 E\,I\,dz & - & - \\ \vdots & \vdots & \ddots & - \\ \int_0^L w''_{\delta 1} w''_{\gamma n} E\,I\,dz & \int_0^L w''_{\gamma 1} w''_{\gamma n} E\,I\,dz & \cdots & \int_0^L w''_{\gamma n}{}^2 E\,I\,dz \end{bmatrix}, \tag{14}$$

in which it is supposed that $EI = E(z)I(z)$.

Remark 3. It is worth noting that if the rotational inertia is taken into account, it is necessary to add the term $\frac{1}{2}\int_0^{L_i} \dot{\psi}_i^2 \rho_i I_i \, dz$ to (6); moreover, in the case of Timoshenko model, it is necessary to add the elastic energy due to shear deformation $\frac{1}{2}\int_0^{L_i} \frac{G_i A_i}{\chi_i}\left(\frac{\partial d_i}{\partial z} - \gamma_i\right)^2 dz$ to (13)

The gravitational potential energy results

$$U_{gi} = g\int_0^{L_i} y_i m(z)dz + M_i^- g y_{o\,i} + M_i^+ g y_i \Big|_{z=L_i} , \tag{15}$$

where g is the gravitational acceleration. By substituting the second of (1) into (15), it results

$$U_g = Mgy_o + Ng\sin\alpha + \left(M^+\delta_n + h^T q_f\right) g\cos\alpha \ , \tag{16}$$

in which the subscript i has been omitted.

Remark 4. It is interesting to note that the matrices B_{fi} and K_i and the vectors h_i and k_i can be easily calculated una tantum in a numerical way (or also analytically in the case of homogeneous links having constant cross-section). Moreover, it is important to note that the matrices B_{fi} and K_i are very sparse (Fig. 7) and also well-conditioned; this fact is in accordance with (9), (14) and with the wavelet nature of the basis functions (Fig. 6).

Instead, when other basis functions, such as the polynomial or the modal ones, are used, the above matrices are full and ill-conditioned.

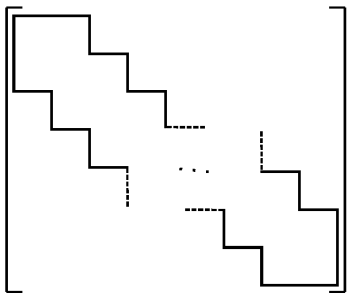

Fig. 7 Structure of the matrices B_{fi} and K_i of the i-th link.

Remark 5. It is worth noting that the compact and closed-form expression of the kinetic energy (7) can be further simplified if the higher order terms $q_f{}^T B_f q_f$ and $M^+\delta_n^2$ are neglected.

Remark 6. It is important to note that if

$$\beta = \frac{GAL^2/\chi}{EI} > 100 \tag{17}$$

the Timoshenko beam theory practically coincides with the Euler-Bernoulli one. For example, for a link made of steel having square hollow constant cross-section, with side $l_i = 40\text{mm}$, thickness $s_i = 2\text{mm}$ and length $L_i = 5\text{m}$, it is $\beta = 2.88 \cdot 10^4$. It follows that, for the majority of flexible robots, it is possible to apply the Euler-Bernoulli beam theory.

II.4 Interconnection algorithm

In this paragraph an algorithm for the calculation of the Lagrangian function of a robot constituted by interconnected flexible links is presented, starting from the results, valid for a single link, stated above.

This algorithm allows to calculate the kinetic and the potential energies of a robot constituted by v flexible links of the type shown in Fig. 2.

The kinetic energy of the *i*-th link (7) can be rewritten in a compact matricial form as follows

$$T_i = \frac{1}{2}\dot{\tilde{q}}_i^T \tilde{B}_i \dot{\tilde{q}}_i, \tag{18}$$

where:

- $\tilde{q}_i^T = \begin{bmatrix} q_{ti}^T & q_i^T \end{bmatrix}$, $q_{ti}^T = \begin{bmatrix} x_{o,i} & y_{o,i} \end{bmatrix}$, $q_i^T = \begin{bmatrix} \alpha_i & q_{fi}^T \end{bmatrix}$; $\tilde{B}_i = \begin{bmatrix} \tilde{B}_{11i} & \tilde{B}_{12i} \\ \tilde{B}_{12i}^T & \tilde{B}_{22i} \end{bmatrix}$,

  $\tilde{B}_{11i} = \begin{bmatrix} M_i & 0 \\ 0 & M_i \end{bmatrix}$;

- $\tilde{B}_{12i} = \begin{bmatrix} -\left(M_i^+ \delta_{in_i} + h_i^T q_{fi}\right)\cos\alpha_i - N_i \sin\alpha_i & -\tilde{h}_i^T \sin\alpha_i \\ -\left(M_i^+ \delta_{in_i} + h_i^T q_{fi}\right)\sin\alpha_i + N_i \cos\alpha_i & \tilde{h}_i^T \cos\alpha_i \end{bmatrix}$;

  $\tilde{B}_{22i} = \begin{bmatrix} J_i + q_{fi}^T B_{fi} q_{fi} + M_i^+ \left(L_i^2 + \delta_{in_i}^2\right) & \tilde{k}_i^T \\ \tilde{k}_i & \tilde{B}_{fi} \end{bmatrix}$;

- $\tilde{h}_i^T$ is obtained by adding M_i^+ to the *(2n$_i$-1)*-th element of vector h_i^T;
- $\tilde{k}_i^T$ is obtained by adding $M_i^+ L_i$ to the *(2n$_i$-1)*-th element and J_i^+ to the *2n$_i$*-th element of vector k_i^T;
- $\tilde{B}_{fi}$ is obtained by adding M_i^+ to the *(2n$_i$-1, 2n$_i$-1)*-th element and J_i^+ to the *(2n$_i$, 2n$_i$)*-th element of the matrix B_{fi}

Now observe that, being the *1*-st link hinged to the base, the variables x_{o1} and y_{o1} do not appear in the kinetic energy expression, hence

$$T_1 = \frac{1}{2}\dot{q}_1^T B_1 \dot{q}_1, \tag{19}$$

where $B_1 = \tilde{B}_{221}$. Moreover, the rigid translation variables $x_{o\,i+1}$ and $y_{o\,i+1}$, $1 \le i \le \nu - 1$ are redundant, since they depend on α_k, δ_{kn}, $k = 1,\ldots,i$; in fact from (1) the following recursive relationship can be derived

$$\begin{bmatrix} \dot{x}_{o\,i+1} \\ \dot{y}_{o\,i+1} \end{bmatrix} = \begin{bmatrix} \dot{x}_{o\,i} \\ \dot{y}_{o\,i} \end{bmatrix} + A_i(\alpha_i, \delta_{in_i}) \begin{bmatrix} \dot{\alpha}_i \\ \dot{q}_{fi} \end{bmatrix}, \tag{20}$$

where $A_i \in R^{2\times(2n_i+1)}$ is given by

$$A_i = \begin{bmatrix} -L_i \sin\alpha_i - \delta_{in}\cos\alpha_i & 0 & .. & 0 & -\sin\alpha_i & 0 \\ L_i \cos\alpha_i - \delta_{in}\sin\alpha_i & 0 & .. & 0 & \cos\alpha_i & 0 \end{bmatrix}. \tag{21}$$

Therefore, equation (18), for $i \ge 2$, can be rewritten as function of the only Lagrangian variables as follows

$$T_i = \frac{1}{2}\dot{q}_{1\ldots i}^T A_{1\ldots i-1}^T \tilde{B}_i A_{1\ldots i-1} \dot{q}_{1\ldots i} = \frac{1}{2}\dot{q}_{1\ldots i}^T B_i \dot{q}_{1\ldots i},\ q_{1\ldots i}^T = \begin{bmatrix} q_1^T & \cdots & q_i^T \end{bmatrix},$$

$$A_{1\ldots i-1} = \begin{bmatrix} A_1 \ldots A_{i-1} & O \\ O & I_{2n_i+1} \end{bmatrix}, \tag{22}$$

in which I_p denotes the identity matrix of order p and O is a zero matrix of suitable dimensions.

Finally, the kinetic energy of the robot constituted by ν flexible links results

$$T = \frac{1}{2}\dot{q}^T B \dot{q}, \tag{23}$$

where $q = q_{1\ldots\nu}$ and the inertia matrix B is obtained "by adding" the matrices B_i according to the recursive scheme reported in Fig. 8.

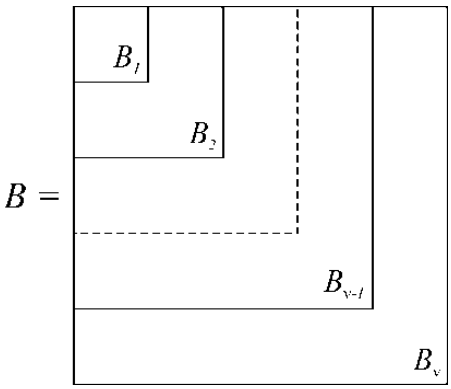

Fig. 8 Composition scheme of the matrix *B*.

Remark 7. It is useful to note that the matrices A_i are very sparse, well-conditioned and they always depend only on the deformation variable δ_{in_i}, whatever the number of Lagrangian deformation variables (i.e of wavelet functions) is, and they do not depend on all the Lagrangian deformation variables, as it happens when other basis functions are used.

Concerning the elastic potential energy of the whole robot, it is easy to verify that it results

$$U_e = \frac{1}{2} q^T K q \,, \tag{24}$$

where the matrix *K* is the following block diagonal matrix

$$K = diag(0, K_1, 0, K_2, \ldots, 0, K_v) \,. \tag{25}$$

Finally, the gravitational potential energy of the whole robot is obtained as the sum of

$$U_{gi} = M_i g \sum_{k=1}^{i-1} \left(L_k \sin\alpha_k + \delta_{kn_k} \cos\alpha_k \right) + \left(m_i \frac{L_i^2}{2} + M_i^+ L_i \right) g \sin\alpha_i + \left(M_i^+ \delta_{in_i} + h_i^T q_{fi} \right) g \cos\alpha_i \,, \quad (26)$$

where U_{gi} is the gravitational potential energy of the *i*-th link.

II.5 Dynamic model of the robot

In this paragraph the dynamic model of the whole robot is considered in the more suitable form presented in [40], [43] by using the Euler-Lagrange method.

It is easy to show that this model, under the assumptions that control actions $C_1 \quad C_2 \quad \cdots \quad C_v$ and disturbances $C_d \quad F_d$ are the ones reported in Fig. 9, results

$$\frac{d}{dt}\left(B(q)\dot{q} \right) - \frac{1}{2}\frac{\partial}{\partial q}\dot{q}^T B(q)\dot{q} + Kq + \frac{\partial}{\partial q}U_g = H_c u_c + H_d u_d \,, \quad (27)$$

where:

$$u_c^T = \left[C_1 \quad C_2 \quad \cdots \quad C_v \right], \; u_d^T = \left[C_d \quad F_d \right], \quad (28)$$

$$H_c = \begin{bmatrix} 1 & -1 & 0 & \cdots \\ O & O & O & \cdots \\ 0 & -1 & 0 & \cdots \\ 0 & 1 & -1 & \cdots \\ O & O & O & \cdots \\ 0 & 0 & -1 & \cdots \\ 0 & 0 & 1 & \cdots \\ O & O & O & \cdots \\ 0 & 0 & 0 & \cdots \\ \vdots & \vdots & \vdots & \ddots \end{bmatrix}, \quad H_d = \begin{bmatrix} h_{d11} & h_{d12} \\ h_{d21} & h_{d22} \\ \vdots & \vdots \\ h_{dv1} & h_{dv2} \end{bmatrix}, \quad (29)$$

in which

$$h_{di1}^T = \begin{bmatrix} 0 & O & 0 & 0 \end{bmatrix},\ i = 1,\ldots,\nu-1,\ h_{d\nu 1}^T = \begin{bmatrix} 1 & O & 0 & 1 \end{bmatrix},$$
$$h_{d\,2}^T = \begin{bmatrix} -L_i \sin(\alpha_i - \alpha_d) - \delta_{in_i} \cos(\alpha_i - \alpha_d) & O & -\sin(\alpha_i - \alpha_d) & 0 \end{bmatrix},\ i = 1,2,\ldots,\nu, \tag{30}$$

being O a zero vector of suitable dimension.

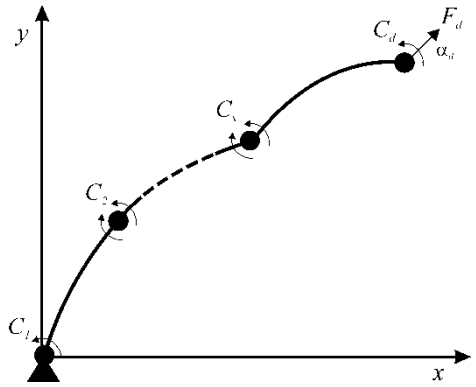

Fig. 9 Control actions and disturbances acting on the robot.

II.6 Validation guidelines

In order to validate the dynamic model of a flexible robot in an efficient and effective way, it is advisable to consider it in significant and realistic operative conditions. The authors propose the following guidelines to validate the model of a flexible robot:

- let be considered the robot in the following conditions: hinged joints, clamped joints, joints controlled with a well-defined and realistic control action of PD type;
- for each of the above cases let be derived the linearized model of the robot around those equilibrium configurations for which some theoretical results exist in literature and/or around those configurations more recurring in

practical applications, considering the gravity action q_g and the disturbances $F_x = F_d \cos\alpha$, $F_y = F_d \sin\alpha$, and $C = C_d$ applied to the end effector as inputs, and the position and the orientation of the end effector as outputs (Fig. 10);

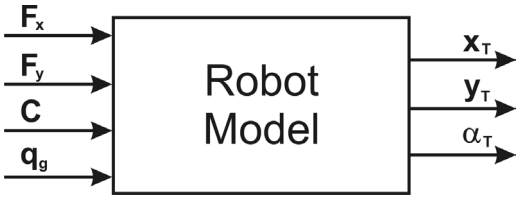

Fig. 10 Input-output scheme of the robot.

- let be derived the global parameters of the obtained models, like static gain, dominant poles and frequency response, and let them be compared with those obtained by using the proposed method, but with a sufficiently high number of wavelet functions per link. This comparison is justified by the fact that, by virtue of the Instantaneity Principle, the proposed method has the property of deriving a model that converges to the exact one starting from low frequencies, without incurring in numerical instability problems;
- let be compared the calculated results with the theoretical ones known in literature, with the ones obtained by increasing the number of the Lagrangian deformation variables, with the ones obtained with other modeling methods proposed in literature;
- let be made suitable dynamic simulations of the flexible robot for assigned nominal inputs when the number of deformation degrees of freedom increases;

- let be evaluated the numerical stability of the model when the number of Lagrangian deformation variables increases, by calculating the condition number of the inertia matrix for the more significant equilibrium configurations.

In the sequel, for the convenience of the reader, some theoretical results known in literature (see e.g. [36]), useful in order to validate the model according to the above guidelines, are reported.

I Hinged link having constant cross-section (Fig. 11):

- Natural frequencies: $f_i = \frac{\lambda_i^2}{2\pi L^2}\sqrt{\frac{EI}{m}},\ i = 1, 2, \ldots$

where

$$\lambda_i = 3.92660231, 7.06858275, 10.21017612, 13.35176878, 16.49336143, (4i+1)\frac{\pi}{4}\ i > 5. \quad (31)$$

- Tip rotation when $q_g = -mg$ and $F = \frac{mgL}{2}$: $\alpha = \frac{mgL^3}{24EI}$.

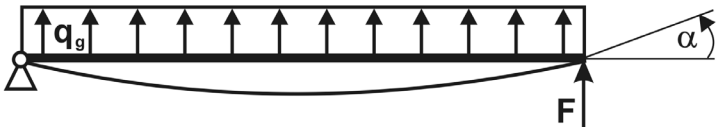

Fig. 11 Static deflection of a hinged link with constant cross-section.

II Clamped link having constant cross-section (Fig. 12):

- Natural frequencies: $f_i = \frac{\lambda_i^2}{2\pi L^2}\sqrt{\frac{EI}{m}}\ , i = 1, 2, \ldots$

where

$$\lambda_i = 1.87510407, 4.69409113, 7.85475744, 10.99554073, 14.13716839, (2i-1)\frac{\pi}{2} \quad i > 5. \quad (33)$$

- Tip vertical deflection δ and tip rotation α :

$$\delta = \begin{cases} \dfrac{FL^3}{3EI} & se\ F \neq 0, C = 0, q_g = 0 \\ \dfrac{CL^2}{2EI} & se\ F = 0, C \neq 0, q_g = 0 \\ \dfrac{q_g L^4}{8EI} & se\ F = 0, C = 0, q_g \neq 0 \end{cases} \quad \alpha = \begin{cases} \dfrac{FL^2}{2EI} & se\ F \neq 0, C = 0, q_g = 0 \\ \dfrac{CL}{EI} & se\ F = 0, C \neq 0, q_g = 0 \\ \dfrac{q_g L^3}{6EI} & se\ F = 0, C = 0, q_g \neq 0 \end{cases} \quad (34)$$

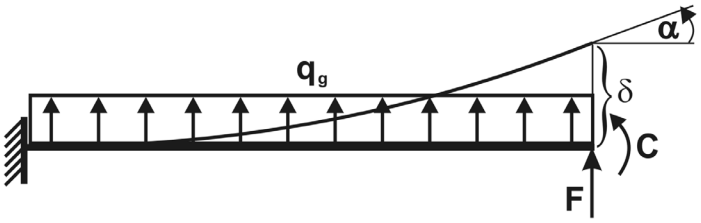

Fig. 12 Static deflection of a clamped link with constant cross-section.

II.7 A methodology to introduce the internal friction

By using the modeling approach based on wavelet functions developed in the above paragraphs, a simple and effective technique has been developed, which allows to introduce friction in the dynamic model of a flexible robot.

Friction is introduced by considering the beam dynamic equation with inertial load and internal friction

$$EI\frac{\partial^4 d}{\partial z^4} - k_a \frac{\partial^3 d}{\partial t \partial z^2} + m\frac{\partial^2 d}{\partial t^2} = 0\,; \quad (35)$$

the work of the non conservative forces is

$$k_a \int_0^L \frac{\partial^3 d}{\partial t \partial z^2} dz \approx k_a \sum_{k=1}^{n} \left(\dot{\delta}_k(t) \int_0^L w''_{\delta k}(z) dz + \dot{\gamma}_k(t) \int_0^L w''_{\gamma k}(z) dz \right). \tag{36}$$

By expanding the above relationship, the internal friction can be modeled with a matricial expression of the type $D\dot{q}_f$.

II.8 Properties of the methodology and illustrative examples

In this paragraph the properties of the proposed modeling methodology and some significant examples are presented.

II.8.1 Static and dynamic precision

The following result holds.

Theorem 1. For any static equilibrium configuration, the position and the orientation of the planar robot constituted by flexible links having constant cross-section calculated with the proposed method (27), at the endpoints of the partition intervals Z_k, both in the presence of gravity actions due to links and payload, and in the presence of concentrated torques and forces control actions and disturbances, strictly coincide with those obtained by using the Euler-Bernoulli beam theory.

Proof. By virtue of the sectioning principle of a structure, without loss of generality, the proof of the theorem is given in the case of a robot constituted by one flexible link in the horizontal configuration and referring to the endpoint Z_n^+; moreover, it is supposed that the link partition is uniform like the one defined in (5). With regard to the case of concentrated forces and torques applied to the tip,

the proof easily follows from the way in which $w_{\delta k}$ and $w_{\gamma k}$ are obtained. With regard to the gravity actions acting on the link, due to the distributed mass, it is worth noting that the corresponding system of generalized forces is the one reported in Fig. 13.

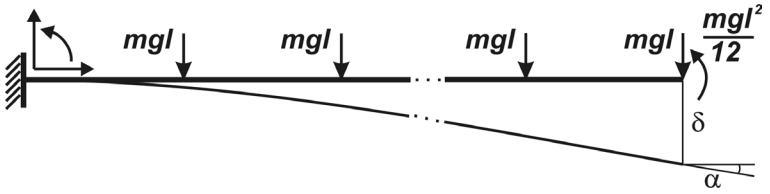

Fig. 13 System of generalized forces equivalent to the gravity action.

From Fig. 13 and from the first and the second of (34) it is

$$\alpha = -\frac{mgl}{2EI}\sum_{i=1}^{n-1}(il)^2 - \frac{mgl(nl)^2}{4EI} + \frac{mgl^2(nl)}{12EI}, \tag{37}$$

ut it results that

$$\sum_{i=1}^{n} i^2 = \frac{n^3}{3} + \frac{n^2}{2} + \frac{n}{6}; \tag{38}$$

in fact, by using the Principle of Induction, it is

$$\sum_{i=1}^{n+1} i^2 = \frac{n^3}{3} + \frac{n^2}{2} + \frac{n}{6} + (n+1)^2 = \frac{n^3}{3} + \frac{n^2}{2} + \frac{n}{6} + \frac{3n^2}{3} + \frac{3n}{3} + \frac{2n}{2} + \frac{1}{3} + \frac{1}{2} + \frac{1}{6} =$$

$$= \frac{(n+1)^3}{3} + \frac{(n+1)^2}{2} + \frac{n+1}{6}.$$

Therefore from (37), by virtue of (38), it is $\alpha = -\frac{mg(nl)^3}{6EI}$, in accord with the (34).

In order to complete the proof, it is worth noting that the vertical tip displacement of a clamped horizontal link subjected to a vertical concentrated force not applied to the tip, as shown in Fig. 14, results

$$\delta = -\frac{Fa^3}{3EI} - \frac{Fa^2 b}{2EI}; \tag{39}$$

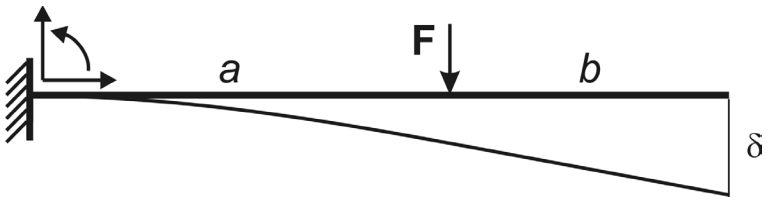

Fig. 14 Link subjected to a vertical concentrated force not applied to the tip.

From Fig. 13 and from (39) it is

$$\delta = -\frac{mgl}{3EI}\sum_{i=1}^{n-1}(il)^3 - \frac{mgl}{2EI}\sum_{i=1}^{n-1}(il)^2(n-i)l - \frac{mgl(nl)^3}{6EI} + \frac{mgl^2(nl)^2}{24EI},$$

which can be rewritten as

$$\delta = \frac{mgl^4}{6EI}\sum_{i=1}^{n-1} i^3 - \frac{mgnl^4}{2EI}\sum_{i=1}^{n-1} i^2 - \frac{mgl(nl)^3}{6EI} + \frac{mgl^2(nl)^2}{24EI}, \tag{40}$$

but, by induction,

$$\sum_{i=1}^{n} i^3 = \frac{n^4}{4} + \frac{n^3}{2} + \frac{n^2}{4}. \tag{41}$$

Therefore from (40), by using (38) and (41), it is $\delta = -\dfrac{mg(nl)^4}{8EI}$, in accord with (34). On this basis, to illustrate the dynamic precision of the proposed method, consider the following example.

Example 1. Let be considered a robot constituted by two flexible links made of aluminium having square hollow constant cross-section (Fig. 15) with length $L_1 = L_2 = 2\text{m}$, side $l_1 = l_2 = 20\text{mm}$, thickness $s_1 = s_2 = 1\text{mm}$, $E_1 = E_2 = 6.4 \cdot 10^{10}\,\text{N/m}^2$, $\rho_1 = \rho_2 = 2.7 \cdot 10^3\,\text{kg/m}^3$.

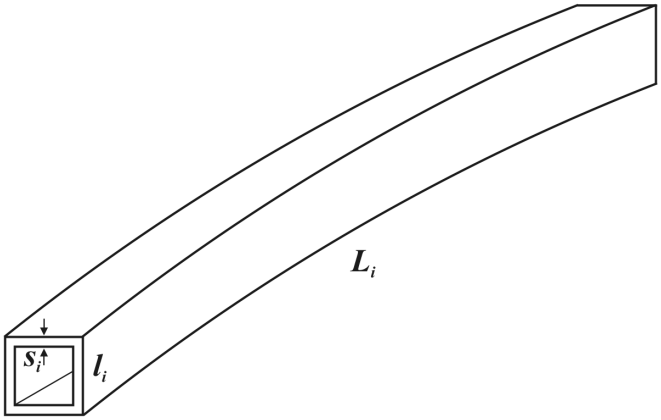

Fig. 15 *I*-th flexible link having square hollow constant cross-section.

Let be considered the above robot in the horizontal configuration with clamped joints. In this configuration the robot can be considered as a single clamped link of length $L_1 + L_2$.

In Table I the first two theoretical frequencies (f_T) obtained from (33), the ones (f_W) obtained with the proposed method with two wavelet functions per link, the ones (f_I) obtained with the assumed mode method by using, for each link, the

first two modes of the clamped-free configuration, the frequencies (f_C) obtained with the assumed mode method by using, for each link, the first two modes of the hinged-free configuration and, finally, the ones (f_P) obtained by using the Ritz-Kantorovich expansion with two deformation polynomials per link are reported.

$f_T(Hz)$	$f_W(Hz)$	$f_I(Hz)$	$f_C(Hz)$	$f_P(Hz)$
1.32	1.32	1.36	1.51	1.32
8.29	8.36	9.28	10.00	8.36

Table I First two frequencies of the robot with clamped links having constant cross-section.

In Table II and in Table III the values of the tip rotation α and of the vertical tip displacement δ produced by an ending torque $C = 10\text{Nm}$, by an ending vertical force $F = 5\text{N}$ and by the gravitational payload are respectively reported; these ones are calculated by using the theoretical formulae (34) and the models of the robot obtained with the various approaches, as above.

	$\alpha_T(\text{deg})$	$\alpha_W(\text{deg})$	$\alpha_I(\text{deg})$	$\alpha_C(\text{deg})$	$\alpha_P(\text{deg})$
C	7.81	7.81	6.26	5.83	7.81
F	7.81	7.81	6.92	6.03	7.81
q_g	4.19	4.19	3.83	3.20	4.19

Table II Tip rotation for concentrated torque and force applied to the tip and for the gravitational payload.

	$\delta_T(\text{mm})$	$\delta_W(\text{mm})$	$\delta_I(\text{mm})$	$\delta_C(\text{mm})$	$\delta_P(\text{mm})$
C	273	273	241	211	273
F	363	363	332	280	363
q_g	219	219	206	167	219

Table III Vertical tip displacement for concentrated torque and force applied to the tip and for the gravitational payload.

From Table I, Table II and Table III it emerges that the proposed method and the Ritz-Kantorovich expansion, which are equivalent in the considered case of links with constant cross-section and for the number of deformation freedom degrees chosen, result better than the ones based on the assumed mode method.

Example 2. Let be considered a robot constituted by two flexible links made of steel having square hollow and piecewice constant cross-section (Fig. 16) with $L_1^+ = L_1^- = L_2^+ = L_2^- = 1.25\text{m}$, $l_1^- = 40\text{mm}$, $l_1^+ = 30\text{mm}$, $l_2^- = 20\text{mm}$, $l_2^+ = 10\text{mm}$, $s_1 = s_2 = 2\text{mm}$, $E_1 = E_2 = 21 \cdot 10^{10}\,\text{N/m}^2$, $\rho_1 = \rho_2 = 7.8 \cdot 10^3\,\text{kg/m}^3$.

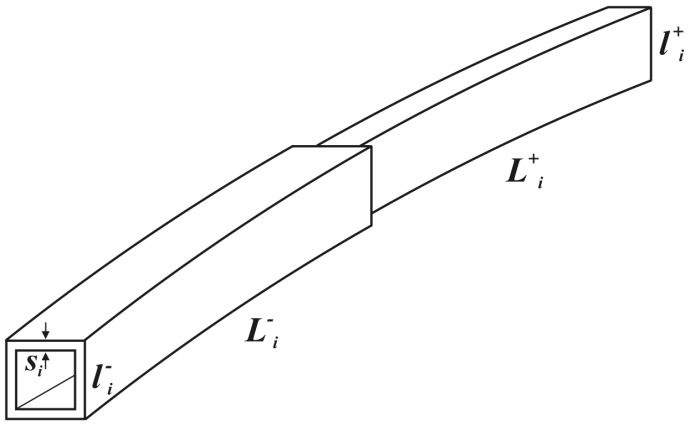

Fig. 16 *I*-th flexible link having square hollow and piecewise constant cross-section.

Let be considered the above flexible robot in the horizontal configuration with joints controlled by a very strong PD action. In Table IV and in Table V the values of the tip rotation $\alpha_T, \alpha_W, \alpha_P$ and of the vertical tip displacement $\delta_T, \delta_W, \delta_P$ produced by an ending torque $C = 50\text{Nm}$, by an ending vertical force $F = 10\text{N}$, and by the gravitational payload are respectively reported. The above

values are calculated by using the proposed method with 20 wavelet functions per link (regarded as the true one), with 2 wavelet functions per link, and the Ritz-Kantorovich expansion with 2 deformation polynomials per link. Moreover, in Fig. 17, Fig. 18 and Fig. 19 the corresponding static deflection are reported. Note that the Theorem 1 is still verified, also if the cross-section is not constant, as it emerges from the reported results.

	α_T(deg)	α_W(deg)	α_P(deg)
C	26.5	26.5	17.2
F	4.32	4.32	2.94
q_g	1.90	1.90	1.45

Table IV Tip rotation for ending torque and force and for gravitational payload.

	δ_T(mm)	δ_W(mm)	δ_P(mm)
C	377	377	257
F	106	106	79
q_g	83	83	73

Table V Vertical tip displacement for ending torque and force and for gravitational payload.

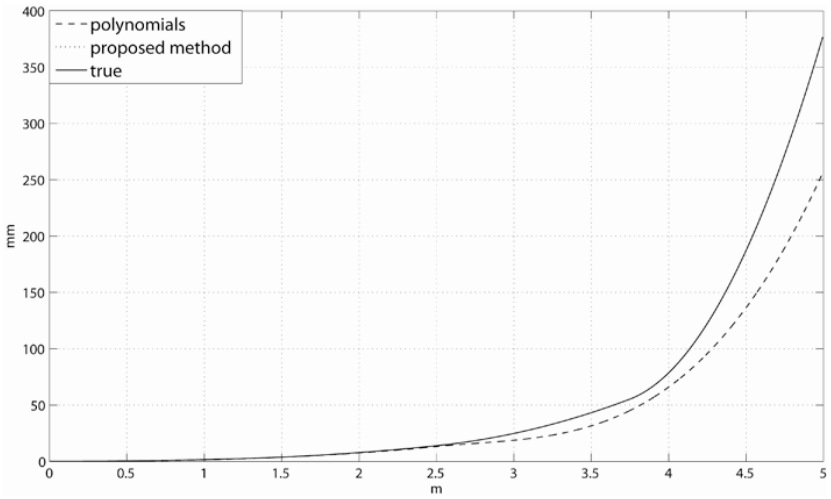

Fig. 17 Static deflection for an ending torque of 50 Nm.

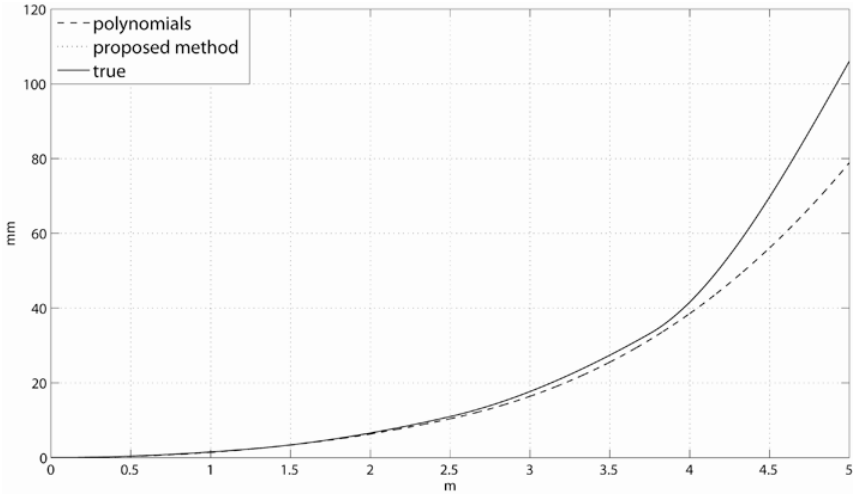

Fig. 18 Static deflection for an ending force of 10 N.

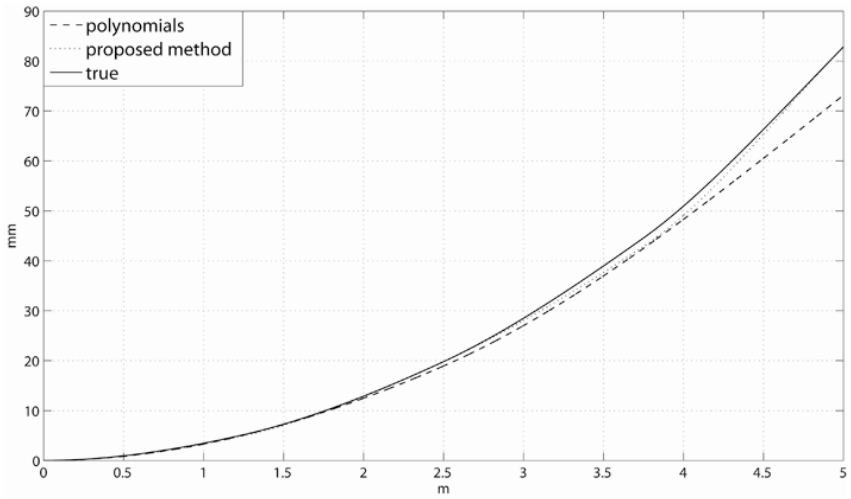

Fig. 19 Static deflection due to the gravity payload.

In Fig. 20 (Fig. 21) the frequency responses ending torque – tip rotation of the robot in the considered configuration are reported, which are obtained by using the proposed method with 10 (20) wavelet functions per link (regarded as the true one), with 2 (4) wavelet functions per link and the Ritz-Kantorovich expansion with 2 (4) deformation polynomials per link. It is worth observing that the frequency range in which the proposed model is reliable widens, starting from the zero frequency, when the number of wavelet functions per link increases.

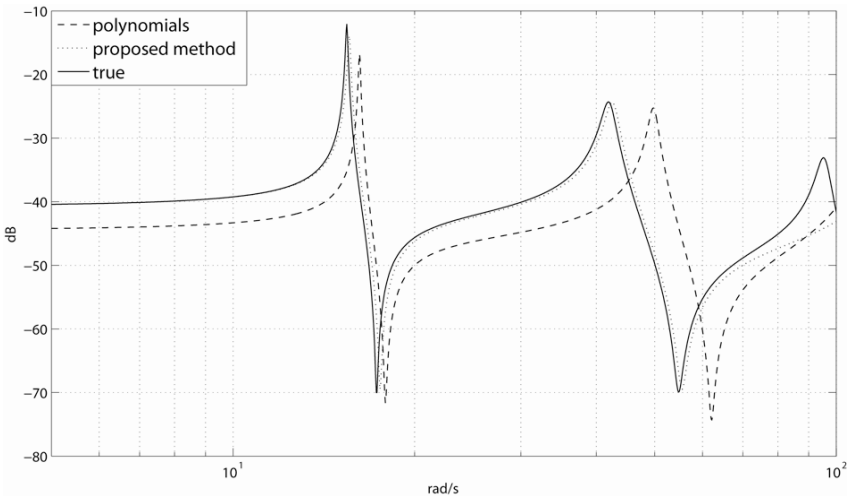

Fig. 20 Frequency responses ending torque – tip rotation of the robot controlled by a strong PD action, with 2 Lagrangian deformation variables per link.

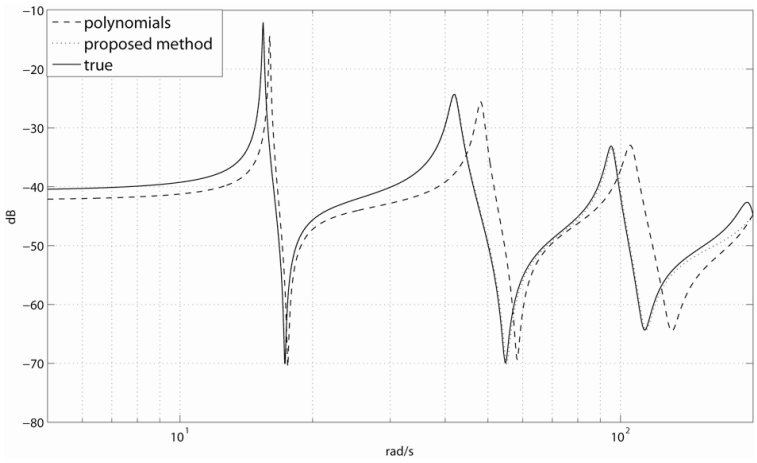

Fig. 21 Frequency responses ending torque – tip rotation of the robot controlled by a strong PD action, with 4 Lagrangian deformation variables per link.

Let be considered the above robot in the horizontal configuration with joints controlled by a weak PD action. In Fig. 22 (Fig. 23) the frequency responses ending torque – tip rotation of the robot in the considered configuration are reported. They are obtained by using the proposed method with 10 (20) wavelet

functions per link (regarded as the true one), with 2 (4) wavelet functions per link and the Ritz-Kantorovich expansion with 2 (4) deformation polynomials per link. It is important to note that, in this case, the first two modes of the controlled robot are due to the rigid motion, whereas the following ones are due to the flexibility and are negligible with respect to the first two modes, i.e. the robot behaviour is practically like a rigid one; this remark shows that the number of Lagrangian deformation variables required to obtain a good model depends, besides on the bandwidth of the command signals and of the disturbances, also on the used control system.

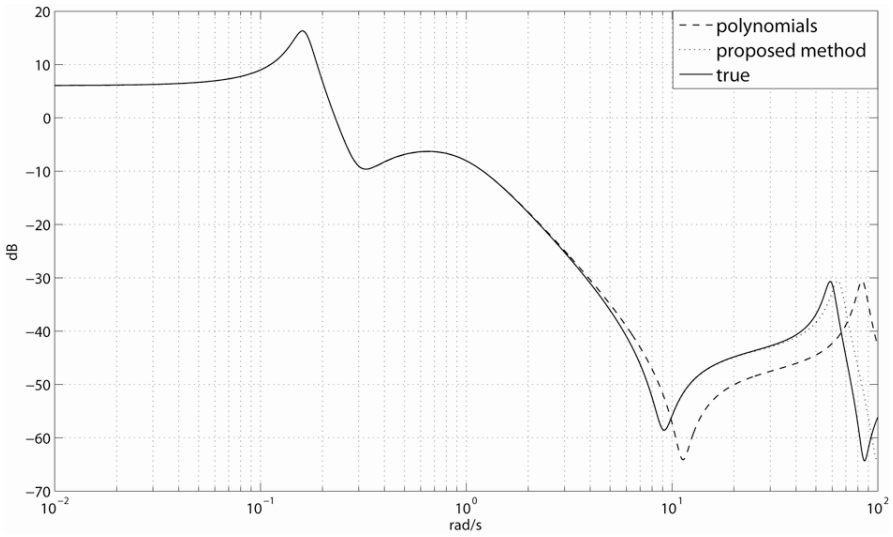

Fig. 22 Frequency responses ending torque – tip rotation of the robot controlled by a weak PD action, with with 2 Lagrangian deformation variables per link.

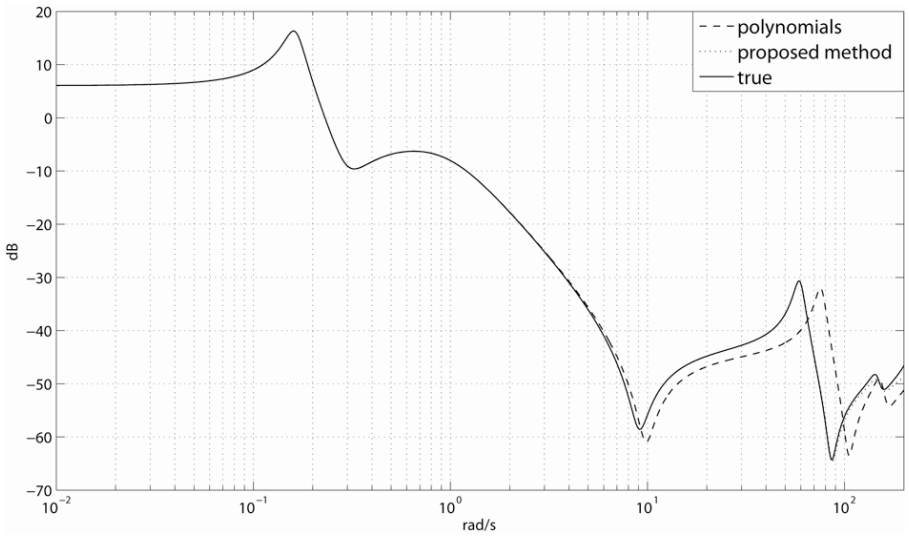

Fig. 23 Frequency responses ending torque – tip rotation of the robot controlled by a weak PD action, with with 4 Lagrangian deformation variables per link.

II.8.2 Numerical stability

The proposed method results numerically very stable with respect to other ones known in literature, in particular the one based on the Ritz-Kantorovich expansion with polynomials, as it clearly emerges from the following example.

Esempio 3. With reference to the robot considered in the Example 1, in Table VI the condition numbers of the inertia matrices calculated with the proposed method and with the Ritz-Kantorovich expansion are reported, for several degrees of the polynomials n_P and numbers of the wavelet functions n_W, such to always consider the same number of deformation freedom degrees n_F per link.

n_F	n_W	n_P	$cond_W$	$cond_P$
2	2	2	$6.16 \cdot 10^3$	$5.48 \cdot 10^4$
6	6	6	$2.35 \cdot 10^5$	$3.68 \cdot 10^{11}$
10	10	10	$1.57 \cdot 10^6$	$2.53 \cdot 10^{18}$

Table VI Condition numbers of the inertia matrices when the number of deformation DOF increases.

For a more global evaluation, according to the proposed guidelines, the frequency responses ending torque – tip rotation of the robot in the considered configuration are reported in Fig. 24. It is worth noting that the frequency response, obtained by using the proposed method with 2 wavelet functions per link, in the considered frequency range practically coincide with the true one, which is still calculated by using the proposed method, but with 20 wavelet functions per link. Finally in Fig. 25 the frequency responses ending torque – tip rotation of the robot in the considered configuration are reported, which are obtained by using the proposed method with 10 and 20 wavelet functions per link and the Ritz-Kantorovich expansion with 10 deformation polynomials per link. It is worth observing that the frequency response obtained with the Ritz-Kantorovich expansion results strongly impaired by the numerical instability, in accord to Table VI and Remark 8.

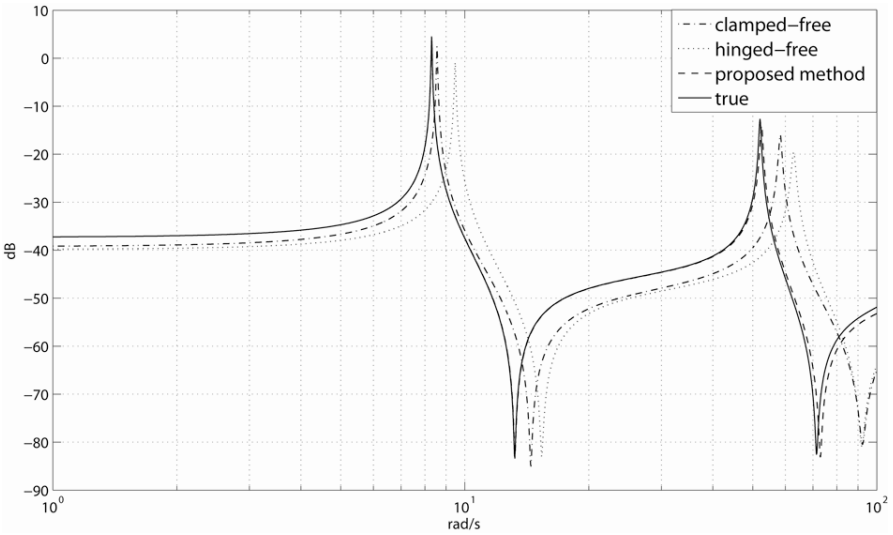

Fig. 24 Frequency responses ending torque – tip rotation with 2 Lagrangian deformation variables per link.

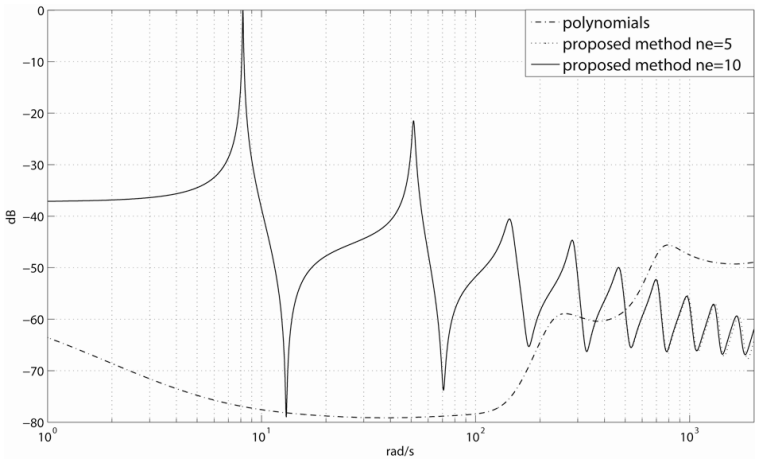

Fig. 25 Frequency responses ending torque – tip rotation with 10 Lagrangian deformation variables per link.

Remark 8. It is explicitly highlighted that, because of the ill-conditioning of the inertia matrix, for $n_p \geq 10$ some eigenvalues of the dynamic matrix of the linearized model of the robot have even positive real part! This is true also in the simple case of a single clamped link robot (Fig. 26). In fact, in this case, the dynamic model, in absence of gravity, results:

$$B\ddot{q} + Kq = Hu, \quad y = H^T q, \tag{42}$$

where:

$$u = \begin{bmatrix} F \\ C \end{bmatrix}, \quad y = \begin{bmatrix} \delta & \alpha \end{bmatrix}, \tag{43}$$

or, in an equivalent way,

$$\dot{x} = \begin{bmatrix} 0 & I \\ -B^{-1}K & 0 \end{bmatrix} x + \begin{bmatrix} 0 \\ B^{-1}H \end{bmatrix} u$$
$$y = \begin{bmatrix} H^T & 0 \end{bmatrix} x. \tag{44}$$

By supposing that $L = 5\text{m}, m = 1\text{kg/m}, EI = 1\text{Nm}^2$ and by using the proposed method with 10 wavelet functions per link, it is easy to verify that:

$$q = \begin{bmatrix} \delta_1 & \gamma_1 & \delta_2 & \gamma_2 & \delta_3 & \gamma_3 & \delta_4 & \gamma_4 & \delta_5 & \gamma_5 \end{bmatrix}^T \tag{45}$$

$$B = \frac{1}{420} \begin{bmatrix} 312 & 0 & 54 & -13 & 0 & 0 & 0 & 0 & 0 & 0 \\ 0 & 8 & 1 & -33 & 0 & 0 & 0 & 0 & 0 & 0 \\ 54 & 13 & 312 & 0 & 54 & -13 & 0 & 0 & 0 & 0 \\ -13 & -3 & 0 & 8 & 13 & -3 & 0 & 0 & 0 & 0 \\ 0 & 0 & 54 & 13 & 312 & 0 & 54 & -13 & 0 & 0 \\ 0 & 0 & -1 & -33 & 0 & 8 & 1 & -33 & 0 & 0 \\ 0 & 0 & 0 & 0 & 54 & 13 & 312 & 0 & 54 & -13 \\ 0 & 0 & 0 & 0 & -1 & -33 & 0 & 8 & 1 & -33 \\ 0 & 0 & 0 & 0 & 0 & 0 & 54 & 13 & 156 & -22 \\ 0 & 0 & 0 & 0 & 0 & 0 & -1 & -33 & -2 & 24 \end{bmatrix}, \tag{46}$$

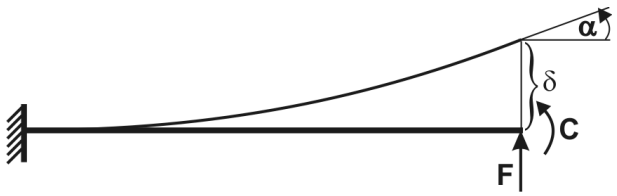

Fig. 26. Single link flexible robot.

$$K=\begin{bmatrix} 2 & 40 & -1 & 26 & 0 & 0 & 0 & 0 & 0 & 0 \\ 0 & 8 & -6 & 2 & 0 & 0 & 0 & 0 & 0 & 0 \\ -1 & -26 & 2 & 40 & -1 & 26 & 0 & 0 & 0 & 0 \\ 6 & 2 & 0 & 8 & -6 & 2 & 0 & 0 & 0 & 0 \\ 0 & 0 & -1 & -26 & 2 & 40 & -1 & 26 & 0 & 0 \\ 0 & 0 & 6 & 2 & 0 & 8 & -6 & 2 & 0 & 0 \\ 0 & 0 & 0 & 0 & -1 & -26 & 2 & 40 & -1 & 26 \\ 0 & 0 & 0 & 0 & 6 & 2 & 0 & 8 & -6 & 2 \\ 0 & 0 & 0 & 0 & 0 & 0 & -1 & -26 & 1 & -26 \\ 0 & 0 & 0 & 0 & 0 & 0 & 6 & 2 & -6 & 4 \end{bmatrix}, \tag{47}$$

$$H=\begin{bmatrix} 0 & 0 & 0 & 0 & 0 & 0 & 0 & 0 & 1 & 0 \\ 0 & 0 & 0 & 0 & 0 & 0 & 0 & 0 & 0 & 1 \end{bmatrix}^T; \tag{48}$$

instead, by using the Ritz-Kantorovich expansion with 10 deformation polynomials, it is easy to verify that:

$$q=\begin{bmatrix} q_{f1} & q_{f2} & q_{f3} & q_{f4} & q_{f5} & q_{f6} & q_{f7} & q_{f8} & q_{f9} & q_{f1} \end{bmatrix}^T, \tag{49}$$

$$B=\left\{\frac{L^{i+j+2}}{i+j+1}\right\}, \quad i=2,3,...,11; j=2,3,...,11, \tag{50}$$

from which:

$$B=\begin{bmatrix} 6.25e2 & 2.60e4 & 1.12e4 & \cdots & 9.39e7 & 4.36e8 \\ 2.60e4 & 1.12e4 & 4.88e4 & \cdots & 4.36e8 & 2.03e9 \\ 1.12e4 & 4.88e4 & 2.17e5 & \cdots & 2.03e9 & 9.54e9 \\ \vdots & \vdots & \vdots & \ddots & \vdots & \vdots \\ 9.39e7 & 4.36e8 & 2.03e9 & \cdots & 2.27e13 & 1.08e14 \\ 4.36e9 & 2.03e9 & 9.54e9 & \cdots & 1.08e14 & 5.18e14 \end{bmatrix}; \tag{51}$$

$$K=\left\{k_{ij}\right\},\quad k_{ij}=\begin{cases}0, & i+j-4<0\\ \dfrac{ij(i-1)(j-1)L^{i+j-3}}{i+j-3}, & i+j-4\geq 0\end{cases},$$

$$i=2,3,...,11;\ j=2,3,...,11, \tag{52}$$

$$H=\begin{bmatrix}L^2 & L^3 & L^4 & \cdots & L^{10} & L^{11}\\ 2L & 3L^2 & 4L^3 & \cdots & 10L^9 & 11L^{10}\end{bmatrix}^T=$$

$$=\begin{bmatrix}25 & 125 & 625 & \cdots & 9765625 & 48828125\\ 20 & 75 & 500 & \cdots & 19531250 & 107421875\end{bmatrix}^T. \tag{53}$$

The condition number of the inertia matrix B (46), obtained with the proposed method, is $7.85\cdot 10^2$, whereas the one of the inertia matrix (51) computed by using the Ritz-Kantorovich expansion is $1.78\cdot 10^{21}$!

Moreover, in the following the exact natural angular frequencies ω_T, calculated by using the theoretic method, the ones calculated by using the proposed method with 10 and 20 wavelet functions, respectively ω_{W10} and ω_{W20}, and finally, due to ill-conditioning problems, the eigenvalues λ_P of the dynamic matrix computed by using the Ritz-Kantorovich expansion are reported:

ω_T =0.1406, 0.8814, 2.4679, 4.8361, 7.9944, 11.9422, 16.6796, 22.2066, 28.5232, 35.6293,

ω_{W10} =0.1406, 0.8818, 2.4768, 4.8928, 8.1208, 13.4909, 19.7305, 28.6136, 40.6478, 59.7951,

ω_{W20}=0.1406, 0.8814, 2.4685, 4.8407, 8.0145, 12.0067, 16.8460, 22.5689, 29.1814, 36.2766,

$\lambda_P = \pm i\,0.1340,\ \pm i\,0.\ 7439,\ \pm i\,1.5938,\ \pm i\,3.377,\ \pm 5.6917,\ \pm i\,10.99,\ \pm i\,28.46,\ \pm 36.99,\ \pm i\,98.28,\ \pm i\,205.57.$

It is worth noting that, because of the ill-conditioning of the inertia matrix (51), obtained by using the Ritz-Kantorovich expansion, some eigenvalues of the dynamic matrix are even positive real!

Esempio 4. Let be considered a robot constituted by two flexible links made of steel, having square hollow and linearly varying cross-section (Fig. 27) with $L_1 = L_2 = 2.5\text{m}$, $l_1^- = 50\text{mm}$, $l_1^+ = 30\text{mm}$, $l_2^- = 30\text{mm}$, $l_2^+ = 10\text{mm}$, $s_1 = s_2 = 2\text{mm}$, $E_1 = E_2 = 21\cdot 10^{10}\,\text{N/m}^2$, $\rho_1 = \rho_2 = 7.8\cdot 10^3\,\text{kg/m}^3$.

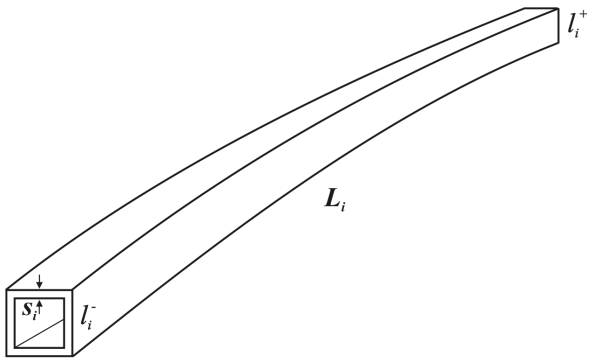

Fig. 27 *I*-th flexible link having square hollow and linearly varying cross-section.

Let be considered the above flexible robot in the horizontal configuration with clamped joints.

In Fig. 28 (Fig. 29) the frequency responses ending torque – tip rotation of the robot in the considered configuration are reported, which are calculated by using the proposed method with 20 wavelet functions per link (regarded as the true one), with 2 (10) wavelet functions per link and the Ritz-Kantorovich expansion with 2 (10) polynomials per link. Also in this case the model obtained with the Ritz-Kantorovich expansion results strongly impaired by numerical instability.

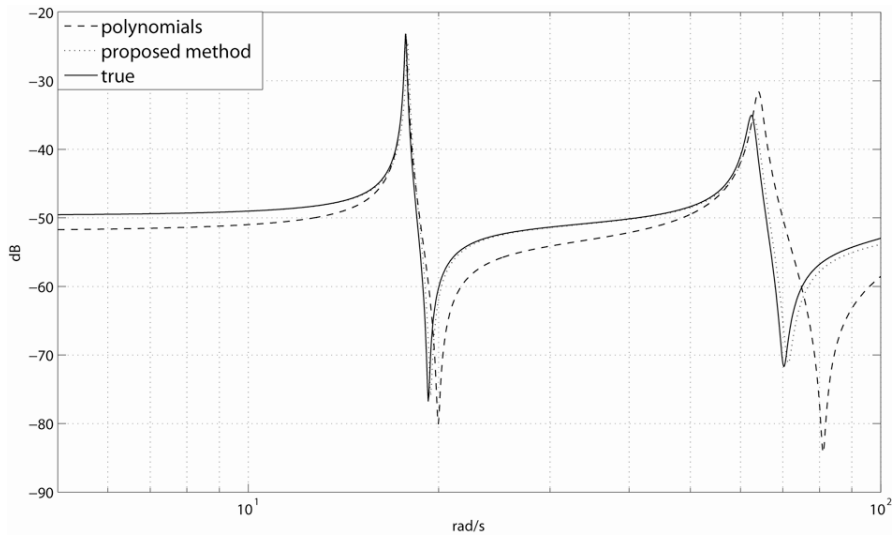

Fig. 28 Frequency responses ending torque – tip rotation with 2 Lagrangian deformation variables per link.

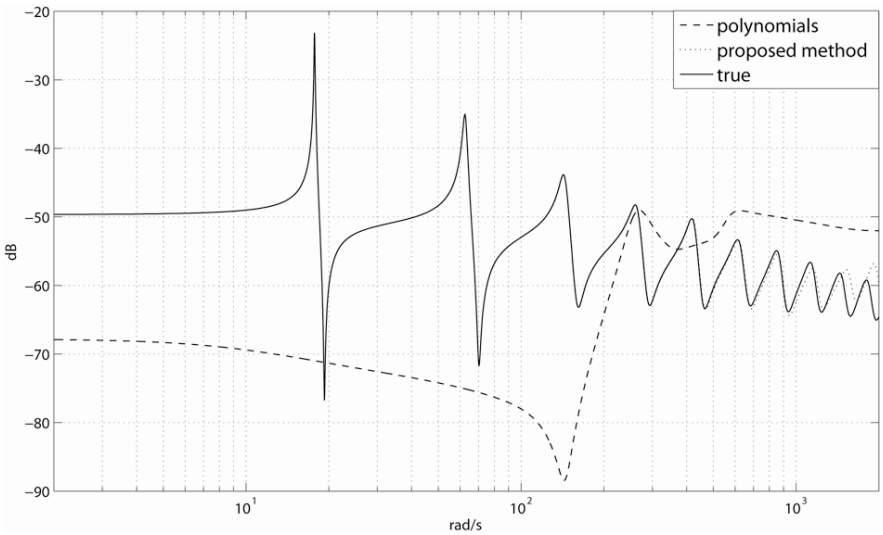

Fig. 29 Frequency responses ending torque – tip rotation with 10 Lagrangian deformation variables per link.

II.8.3 Computational efficiency

By virtue of the sparseness of the matrices B and A_i (Remark 4 and 7) the proposed method results computationally very efficient, as it emerges from the following example.

Esempio 3. S Let be considered a robot constituted by three flexible links having square hollow constant cross-section with parameters $L_1 = L_2 = L_3 = 2.5\text{m}$, $l_1 = l_2 = l_3 = 50\text{mm}$, $s_1 = s_2 = s_3 = 2\text{mm}$, $E_1 = E_2 = E_3 = \quad = 21 \cdot 10^{10}\,\text{N/m}^2$, $\rho_1 = \rho_2 = \rho_3 = = 7.8 \cdot 10^3\,\text{kg/m}^3$. Let be further supposed that (Fig. 2) $M_1^+ = M_2^+ = M_3^+ = M_1^- = \ = M_2^- = M_3^- = 1kg$, $J_1^+ = J_2^+ = J_3^+ = J_1^- = J_2^- = J_3^- = 1\text{kg} \cdot \text{m}^2$.

In Table VII and Table VIII the number of multiplications required to evaluate the inertia matrix B and the gradient of the kinetic energy c are reported, which are

computed by using the various methods, under the assumption that the number of Lagrangian deformation variables per link is 4 (4 polynomials, 4 modes, 4 wavelet functions) and 8 (8 polynomials, 8 modes, 8 wavelet functions) respectively.

	B	c	B and c
Proposed method	344	878	1222
Polynomials	1147	2770	3917
Clamped-free modes	1179	2830	4009
Hinged-free modes	1001	2526	3527

Table VII Number of multiplications with 4 deformation variables per link.

	B	c	B and c
Proposed method	687	1712	2399
Polynomials	4232	10915	15147
Clamped-free modes	4101	10997	15098
Hinged-free modes	3665	10050	13615

Table VIII Number of multiplications with 8 deformation variables per link.

Remark 9. It is worth noting that when the number of Lagrangian deformation variables has doubled also the number of multiplications required by the proposed method has about doubled, instead, the one required by the other methods has about quadrupled.

In Table IX the time costs required by the dynamic simulation of the above robot are reported, in the hypotheses that:

- 4 Lagrangian deformation variables per link are used;
- each joint of the robot is controlled by using a PD controller with $K_p = 5 \cdot 10^3$, $K_d = 250$;

- the torque disturbance $d(t) = 1 \cdot 10^3 \left[1(t-3) - 1(t-4) \right]$ acts on the first joint;
- the initial configuration of the link is undeformed with angles: $\alpha_1 = -20\,\text{deg}$, $\alpha_2 = 0\,\text{deg}$, $\alpha_3 = -20\,\text{deg}$;
- the numerical solver Matlab® ode15s is used, with variable step size and relative tolerance of 10^{-5}.

Proposed method	26.4 s
Polynomials	83.9 s
Clamped-free modes	95.1 s
Hinged-free modes	146.8 s

Table IX Time costs of the dynamic simulation with 4 Lagrangian deformation variables per link.

In Table X the time costs required by the dynamic simulation of the above robot are reported, under the same assumptions as above, but by using 6 Lagrangian deformation variables per link.

Proposed method	124.6 s
Polynomials	18 days(estimated)
Clamped-free modes	648.5 s
Hinged-free modes	722.7 s

Table X Time costs of the dynamic simulation with 6 Lagrangian deformation variables per link.

It is interesting to note that, when the polynomials of the Ritz-Kantorovich expansion are used, the time cost required by the dynamic simulation, which has been estimated on the basis of a shorter simulation, is practically prohibitive. The same result is obtained also if the relative tolerance is 10^{-4}. This fact and the

warnings messages, due to ill-conditioning of the inertia matrix, displayed by the Matlab solver during the simulation, make the the Ritz-Kantorovich expansion practically inapplicable.

In Table XI the time costs required by the dynamic simulation of the above robot are reported, under the same assumptions as above, but supposing that 8 Lagrangian deformation variables per link are used.

Proposed method	504.1 s
Polynomials	775 days (estimated)
Clamped-free modes	4312.4 s
Hinged-free modes	5254.3 s

Table XI Time costs of the dynamic simulation with 8 Lagrangian deformation variables per link.

It is worth noting that, in this case, the simulation is practically possible only with the proposed method, even if the relative tolerance is 10^{-4} or 10^{-3}.

With reference to the last simulation, the plots of the ending deflections δ_i and of the ending rotations γ_i of each link, obtained with the proposed method, are reported in Fig. 30, Fig. 31 and Fig. 32

In conclusion, from the above comparisons it emerges that the simulation times required by the other models are markedly longer than those required by the proposed method as shown in the above tables, both because, due to numerical instability problems, a very small integration step is sometimes required, and because the calculation of the inertia matrix B and of the gradient of the kinetic energy c is very much cumbersome, as it is clear from Table VII and Table VIII.

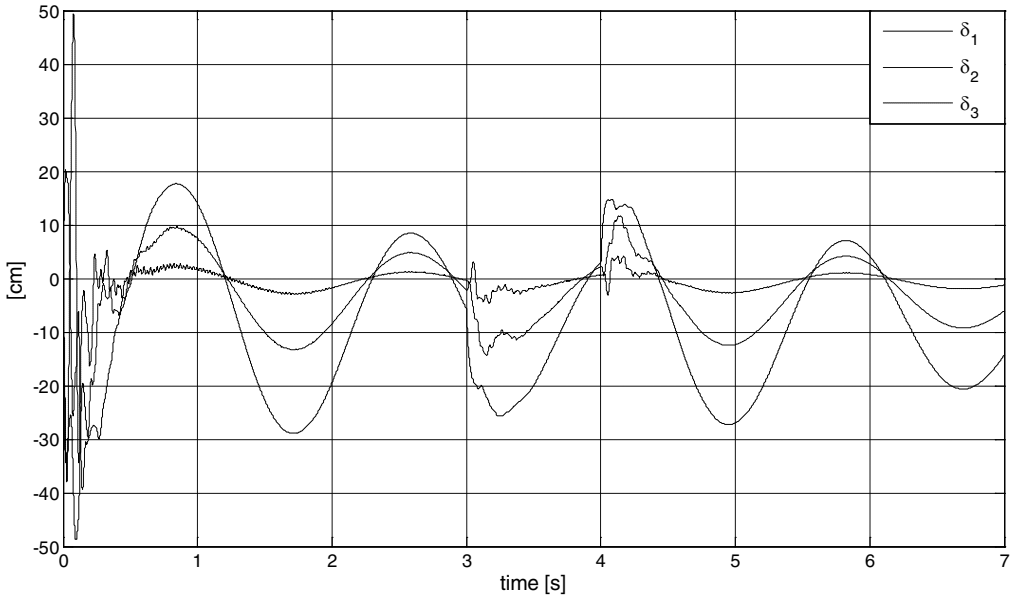

Fig. 30 Time histories of the terminal deflections δ_i of the three links.

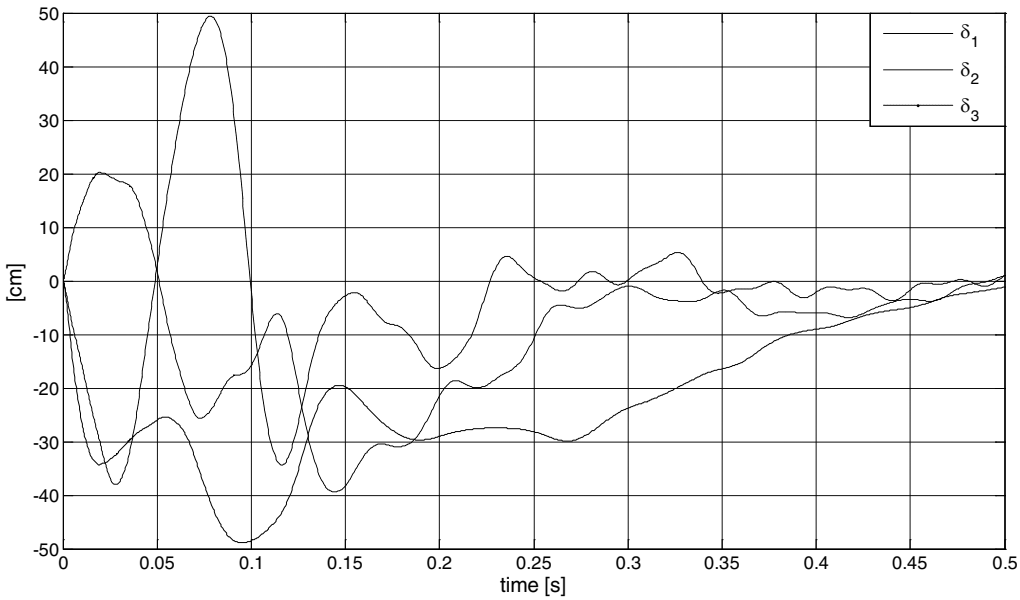

Fig. 31 A detail of Fig. 30.

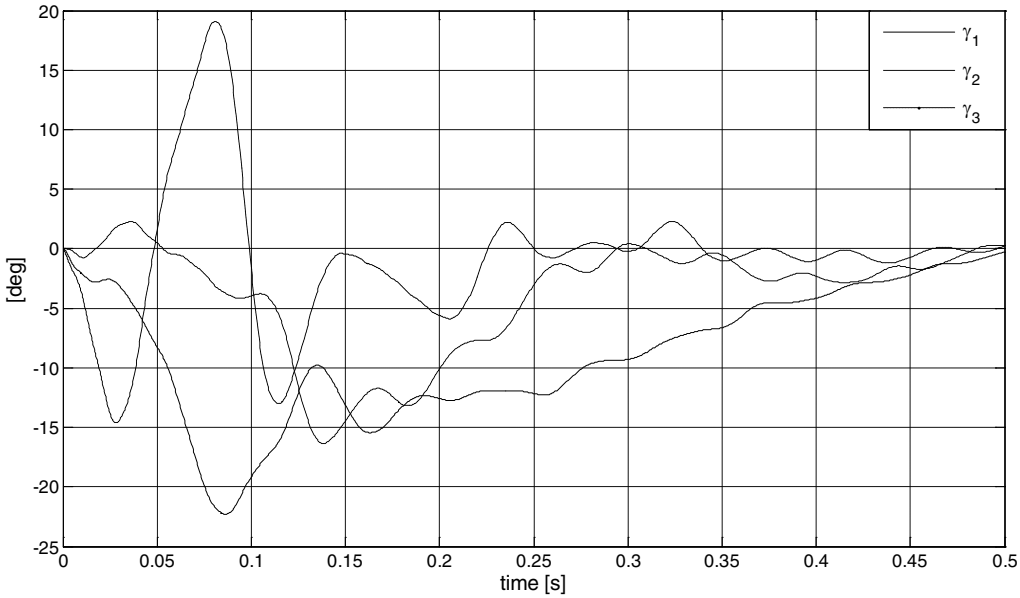

Fig. 32 A detail of the time histories of the terminal rotations γ_i of the three links.

CHAPTER III - A VERY EFFICIENT VARIATION TO THE ASSUMED MODE METHOD

III.1 Introduction

In this chapter a variation to the assumed mode method is presented which allows to obtain the analytical model of a flexible robot and which results drastically more efficient, from a computational point of view, than the classic assumed modes method.

The presented method consists in using suitable linear combinations of the modes of each link as basis functions to evaluate the deflection, such a way to minimize the dependency of the position of the generic link on the Lagrangian variables of the previous links. In this way, the number of terms of the inertia matrix and of the Coriolis and centrifugal vectors is drastically reduced.

The model is derived by firstly analytically calculating, if the links are homogeneous and with constant cross-section, or otherwise by numerically calculating, the parameters of the closed-form expression of the Lagrangian function of the generic link supposed free; afterwards, the analytical dynamic model of the whole robot is obtained by using an iterative interconnection algorithm, which can be easily implemented by using a symbolic manipulation language.

The simplicity and the efficiency of the proposed method is shown with very significant examples.

The results presented in this chapter are based on [47].

III.2 Hypotheses, notations and preliminaries

In this chapter it is considered, for simplicity and for brevity, the case of planar robots with fixed base, constituted by ν flexible links having a straight line as unstressed configuration, both rigid ends of negligible dimensions with respect to its length, and rotation axes orthogonal to the vertical plane. In Fig. 33 a representation of the *i*-th link in the stressed and unstressed configuration is shown.

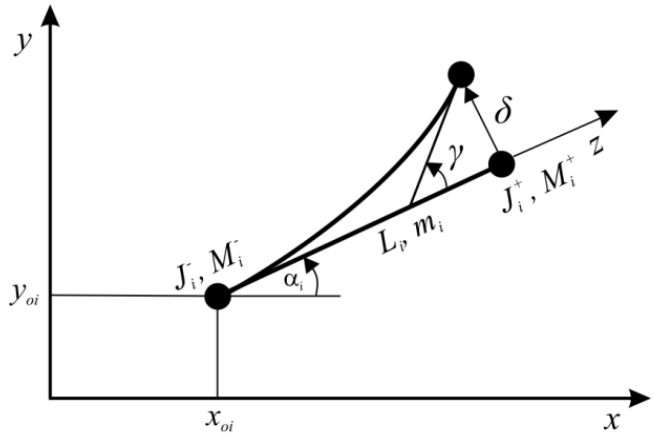

Fig. 33 Schematic representation of a flexible link.

The following preliminary notations are introduced for the generic *i*-th link:

- L_i is the length of the link;
- E_i is the Young's modulus for the flexible part of the link;
- I_i is the area moment of inertia for the cross-section of the link;
- m_i is the mass per unit length of the flexible part of the link;
- M_i^-, M_i^+ are the masses of both rigid ends of the link;

- J_i^-, J_i^+ are the inertia moments of both rigid ends of the link with respect to rotation axes;
- x_{oi}, y_{oi}, α_i are the absolute motion coordinates of the link supposed rigid;
- $d_i(z,t)$ is the vertical deflection of the link in relative coordinates.

III.3 Lagrangian function of a flexible link

In this paragraph the Lagrangian function of a flexible link is obtained.

By using the above notations, the coordinates (x_i, y_i) of a generic point of the *i*-th deflected link can be expressed as:

$$\begin{aligned} x_i &= x_{oi} + z\cos\alpha_i - d_i \sin\alpha_i \\ y_i &= y_{oi} + z\sin\alpha_i + d_i \cos\alpha_i. \end{aligned} \tag{54}$$

The assumed mode method approximates the deflection $d_i(z,t)$ as

$$d_i(z,t) \approx \sum_{k=1}^{n_i} \eta_k(t)\psi_k(z) \tag{55}$$

by using as functions $\psi_k(z)$ the modes deriving from the solution of the Euler-Bernoulli beam equation with distributed inertial load

$$\frac{\partial^2 d}{\partial z^2}\left(EI \frac{\partial^2 d(z,t)}{\partial z^2} \right) + m\frac{\partial^2 d(z,t)}{\partial t^2} = 0. \tag{56}$$

The above modes can be easily analytically computed if $EI = const$; otherwise they can be numerically computed by using standard software packages or by using the method proposed in the previous chapter.

By taking the derivatives of (54) and by using (55), the velocity vector components of a generic point along the deformed link are obtained

$$\begin{aligned}\dot{x}_i &= \dot{x}_{o\,i} - z\sin(\alpha_i)\dot{\alpha}_i - \sum_{k=1}^{n_i}\dot{\eta}_k\psi_k\sin(\alpha_i) - \sum_{k=1}^{n_i}\eta_k\psi_k\cos(\alpha_i)\dot{\alpha}_i \\ \dot{y}_i &= \dot{y}_{o\,i} + z\cos(\alpha_i)\dot{\alpha}_i + \sum_{k=1}^{n_i}\dot{\eta}_k\psi_k\cos(\alpha_i) - \sum_{k=1}^{n_i}\eta_k\psi_k\sin(\alpha_i)\dot{\alpha}_i\end{aligned} \tag{57}$$

where the dependency on z and on t has been omitted for simplicity and n_i is the number of Lagrangian deformation variables of the i-th link.
The kinetic energy of the i-th link can be computed as follows

$$\begin{aligned}T_i = \frac{1}{2}m_i\int_0^{L_i}(\dot{x}_i^2+\dot{y}_i^2)dz + \frac{1}{2}M_i^-(\dot{x}_{o\,i}^2+\dot{y}_{o\,i}^2) + \frac{1}{2}J_i^-\dot{\alpha}_i^2 + \frac{1}{2}M_i^+(\dot{x}_i^2\big|_{z=L_i} + \dot{y}_i^2\big|_{z=L_i}) + \\ + \frac{1}{2}J_i^+\left(\dot{\alpha}_i + \sum_{k=1}^{n_i}\dot{\eta}_k\psi'_k\big|_{z=L_i}\right)^2.\end{aligned} \tag{58}$$

By substituting (57) into (58), after some tedious manipulations and by omitting, for the simplicity of notations, the subscript i, it is

$$\begin{aligned}T = \frac{1}{2}\Big\{M\left(\dot{x}_o^2+\dot{y}_o^2\right) + M^+\left(\mathrm{m}_f^T(L)\dot{q}_f\right)^2 + J^+\left(\mathrm{m}_f'^T(L)\dot{q}_f\right)^2 + \left(J + q_f^T B_f q_f + M^+\left(L^2 + \left(\mathrm{m}_f^T(L)q_f\right)^2\right)\right)\dot{\alpha}^2 + \\ + \dot{q}_f^T B_f\dot{q}_f + 2\left(k^T\dot{q}_f + J^+\mathrm{m}_f'^T(L)\dot{q}_f + M^+L\mathrm{m}_f^T(L)\dot{q}_f\right)\dot{\alpha} - 2\left(M^+\mathrm{m}_f^T(L)q_f + h^Tq_f\right)\dot{\alpha}\left(\dot{x}_o\cos\alpha + \dot{y}_o\sin\alpha\right) + \\ + 2\left(N\dot{\alpha} + h^T\dot{q}_f + M^+\mathrm{m}_f^T(L)\dot{q}_f\right)\left(\dot{y}_o\cos\alpha - \dot{x}_o\sin\alpha\right)\Big\},\end{aligned} \tag{59}$$

where:

- $M = M^- + mL + M^+$, $J = J^- + m\dfrac{L^3}{3} + J^+$, $N = M^+L + \dfrac{1}{2}mL^2$;
- the matrix $B_f \in R^{n\times n}$ is derived by using the relationship

$$\frac{1}{2}m\int_0^L \left(\mathrm{m}_f^T\dot{q}_f\right)^2 dz = \frac{1}{2}\dot{q}_f^T B_f \dot{q}_f \ ; \tag{60}$$

- the vector $h \in R^n$ is derived by using the relationship

$$m\int_0^L \mathrm{m}_f^T\dot{q}_f dz = h^T\dot{q}_f \ ; \tag{61}$$

- the vector $k \in R^n$ is derived by using the relationship

$$m\int_0^L \mathrm{m}_f^T\dot{q}_f z dz = k^T\dot{q}_f \ ; \tag{62}$$

- $q_f \in R^n$ represents the vector of the Lagrangian deformation variables

$$q_f^T = \begin{bmatrix}\eta_1 & \eta_2 & \cdots & \eta_n\end{bmatrix}, \tag{63}$$

- $\mathrm{m}_f(z) \in R^n$ represents the vector of the spatial deformation modes

$$\mathrm{m}_f^T = \begin{bmatrix}\psi_1 & \psi_2 & \cdots & \psi_n\end{bmatrix} . \tag{64}$$

Remark 10. It is worth noting that the matrix B_f and the vectors h and k can be computed off-line, una tantum, for each link and the kinetic energy of the *i*-th link (59) can be conveniently rewritten in a compact matricial form as

$$T_i = \frac{1}{2}\dot{\tilde{q}}_i^T \tilde{B}_i \dot{\tilde{q}}_i , \tag{65}$$

where:

- $\tilde{q}_i^T = \begin{bmatrix} \tilde{q}_{li}^T & q_{li}^T \end{bmatrix}$, $\tilde{q}_{li}^T = \begin{bmatrix} x_{oi} & y_{oi} \end{bmatrix}$, $q_{li}^T = \begin{bmatrix} \alpha_i & q_{fi}^T \end{bmatrix}$; $\tilde{B}_i = \begin{bmatrix} \tilde{B}_{11i} & \tilde{B}_{12i} \\ \tilde{B}_{12i}^T & \tilde{B}_{22i} \end{bmatrix}$;
- $\tilde{B}_{11i} = \begin{bmatrix} M_i & 0 \\ 0 & M_i \end{bmatrix}$, $\tilde{B}_{12i} = \begin{bmatrix} -\left(M_i^+ \mathrm{m}_{fi}^T(L_i) q_{fi} + h_i^T q_{fi}\right)\cos\alpha_i - N_i \sin\alpha_i & -\tilde{h}_i^T \sin\alpha_i \\ -\left(M_i^+ \mathrm{m}_{fi}^T(L_i) q_{fi} + h_i^T q_{fi}\right)\sin\alpha_i + N_i \cos\alpha_i & \tilde{h}_i^T \cos\alpha_i \end{bmatrix}$;
- $\tilde{B}_{22i} = \begin{bmatrix} J_i + q_{fi}^T B_{fi} q_{fi} + M_i^+ \left(L_i^2 + \left(\mathrm{m}_{fi}^T(L_i) q_{fi}\right)^2\right) & \tilde{k}_i^T \\ \tilde{k}_i & \tilde{B}_{fi} \end{bmatrix}$;
- $\tilde{h}_i^T = h_i^T + M_i^+ \mathrm{m}_{fi}^T(L_i)$;
- $\tilde{k}_i^T = k_i^T + J_i^+ \mathrm{m}'^T_{fi}(L_i) + M_i^+ L_i \mathrm{m}_{fi}^T(L_i)$;
- $\tilde{B}_{fi} = B_{fi} + M_i^+ \mathrm{m}_{fi}(L_i)\mathrm{m}_{fi}^T(L_i) + J_i^+ \mathrm{m}'_{fi}(L_i)\mathrm{m}'^T_{fi}(L_i)$.

Once the kinetic energy has been derived, it is necessary to calculate the elastic potential energy U_{ei} and the gravitational potential one U_{gi} of the *i*-th link. The elastic potential energy due to the deformation of the *i*-th link results

$$U_{ei} = \frac{1}{2} E_i I_i \int_0^{L_i} \left(\mathrm{m}''^T_{fi} q_{fi}\right)^2 dz = \frac{1}{2} q_{fi}^T K_i q_{fi}. \tag{66}$$

The gravitational potential energy results

$$U_{gi} = mg \int_0^{L_i} y_i dz + M_i^- g y_{oi} + M_i^+ g y_i \Big|_{z=L_i}, \tag{67}$$

where g is the gravity acceleration. By substituting the second of (54) into (67) and by using (55) it is

$$U_{g\,i} = M_i g y_{o\,i} + N_i g \sin\alpha_i + \left(M_i^{+} \mathrm{m}_{f\,i}^{T}(L_i) q_{f\,i} + h_i^{T} q_{f\,i} \right) g \cos\alpha_i \,. \tag{68}$$

Remark 11. Let be noted that, by virtue of the choice which has been made of the Lagrangian deformation variables, the contribute to the kinetic energy and to the gravitational potential one of the ending inertias M^{+} and J^{+} depends on all the Lagrangian deformation variables of the vector q_f.

III.4 Interconnection algorithm and Lagrangian function of the robot

In this paragraph an algorithm for the calculation of the Lagrangian function of a robot constituted by several interconnected flexible links is presented, starting from the results, valid for a single link, stated in the previous paragraph.

This algorithm allows to calculate the kinetic and the potential energies of a robot constituted by v flexible links having kinetic energy given by (59), elastic potential energy given by (66), and gravitational potential one given by (68).

It is useful to observe that, being the *1*-st link hinged to the base, the variables x_{o1} and y_{o1} do not appear in the kinetic energy expression, hence

$$T_1 = \frac{1}{2} \dot{q}_{l1}^{T} B_1 \dot{q}_{l1}\,, \tag{69}$$

where $B_1 = \tilde{B}_{221}$. Moreover, the rigid translation variables x_{oi} and y_{oi}, $2 \le i \le \nu$ depend on α_k, q_{fk}, $k = 1,\ldots,i-1$; in fact from equations (57) the following recursive relationship can be derived

$$\begin{bmatrix} \dot{x}_{oi+1} \\ \dot{y}_{oi+1} \end{bmatrix} = \begin{bmatrix} \dot{x}_{oi} \\ \dot{y}_{oi} \end{bmatrix} + A_i(\alpha_i, q_{fi}) \begin{bmatrix} \dot{\alpha}_i \\ \dot{q}_{fi} \end{bmatrix}, \tag{70}$$

where $A_i \in R^{2\times(n_i+1)}$ has the following expression

$$A_i = \begin{bmatrix} -L_i \sin\alpha_i - \mathrm{m}_{fi}^T(L_i) q_{fi} \cos\alpha_i & -\sin\alpha_i \mathrm{m}_{fi}^T(L_i) \\ L_i \cos\alpha_i - \mathrm{m}_{fi}^T(L_i) q_{fi} \sin\alpha_i & \cos\alpha_i \mathrm{m}_{fi}^T(L_i) \end{bmatrix}. \tag{71}$$

Therefore, equation (65), for $i \ge 2$, can be rewritten as function of the only Lagrangian variables as follows

$$\begin{aligned} &T_i = \frac{1}{2} \dot{q}_{1\ldots i}^T A_{1\ldots i-1}^T \tilde{B}_i A_{1\ldots i-1} \dot{q}_{1\ldots i} = \frac{1}{2} \dot{q}_{1\ldots i}^T B_i \dot{q}_{1\ldots i}, \; q_{1\ldots i}^T = \begin{bmatrix} q_{l1}^T & \cdots & q_{li}^T \end{bmatrix}, \\ &A_{1\ldots i-1} = \begin{bmatrix} A_1 \ldots A_{i-1} & O \\ O & I_{n_i+1} \end{bmatrix}, \end{aligned} \tag{72}$$

in which I_p denotes the identity matrix of order p and O is a zero matrix of suitable dimensions.

Finally, the kinetic energy of the robot constituted by ν flexible links results

$$T = \frac{1}{2} \dot{q}^T B \dot{q}, \tag{73}$$

where $q = q_{1...v}$ and the inertia matrix B is obtained "by adding" the matrices B_i according to the recursive scheme reported in Fig. 34.

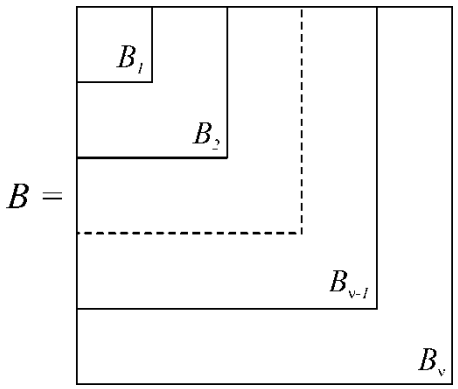

Fig. 34 Composition scheme of the matrix *B*.

Remark 12. It is important to note that, by virtue of the Lagrangian deformation variables chosen, the transformation matrix A_i depends on all the Lagrangian deformation variables of the vector q_f. The above consideration and Remark 10 make the inertia matrix of the robot *B* and the vector *c* of Coriolis and centrifugal terms very burdensome to compute because of the explosive number of their terms, which notably increases when the number of the Lagrangian deformation variables of each link increases.

Concerning the elastic potential energy of the whole robot, it is easy to verify that it results

$$U_e = \frac{1}{2} q^T K q \,, \tag{74}$$

where the matrix *K* is the block diagonal matrix $K = diag(0, K_1, 0, K_2, \ldots, 0, K_v)$.

Finally, the gravitational potential energy of the whole robot U_g is obtained as the sum of

$$U_{gi} = M_i g \sum_{k=1}^{i-1} \left(L_i \sin\alpha_i + \mathrm{m}_{fi}^T(L_i) q_{fi} \cos\alpha_i \right) + N_i g \sin\alpha_i + \left(M_i^+ \mathrm{m}_{fi}^T(L_i) q_{fi} + h_i^T q_{fi} \right) g \cos\alpha_i , \quad (75)$$

where U_{gi} is the gravitational potential energy of the *i*-th link, which has been obtained from (68) by expressing y_{oi} as function of the Lagrangian deformation variables.

Remark 13. It is useful to note that, once the kinetic and potential energies of the generic flexible link have been calculated in a hybrid symbolic-numeric form, the ones of the whole robot can be obtained by implementing the proposed interconnection algorithm with a symbolic manipulation software language.

III.5 Dynamic model of the robot

In this paragraph the dynamic model of the whole robot is derived in the more in [40], [43] by using the Euler-Lagrange method.

It is easy to show that this model, under the assumptions that the control actions $C_1 \quad C_2 \quad \dots \quad C_v$ and the disturbances $C_d \quad F_d$ are the ones reported in Fig. 35, results

$$\frac{d}{dt}\left(B(q)\dot{q} \right) - \frac{1}{2}\frac{\partial}{\partial q}\dot{q}^T B(q)\dot{q} + Kq + \frac{\partial}{\partial q} U_g = H_c u_c + H_d u_d , \quad (76)$$

where:

$$u_c^T = \begin{bmatrix} C_1 & C_2 & \cdots & C_v \end{bmatrix}, \; u_d^T = \begin{bmatrix} C_d & F_d \end{bmatrix}, \quad (77)$$

$$H_c = \begin{bmatrix} 1 & -1 & 0 & \cdots \\ O & -\mathrm{m}'_{f1}(L) & O & \cdots \\ 0 & 1 & -1 & \cdots \\ O & O & -\mathrm{m}'_{f2}(L) & \cdots \\ 0 & 0 & 1 & \cdots \\ O & O & O & \cdots \\ 0 & 0 & 0 & \cdots \\ O & O & O & \cdots \\ 0 & 0 & 0 & \cdots \\ \vdots & \vdots & \vdots & \ddots \end{bmatrix}, \quad H_d = \begin{bmatrix} h_{d11} & h_{d12} \\ h_{d21} & h_{d22} \\ \vdots & \vdots \\ h_{dv1} & h_{dv2} \end{bmatrix}, \tag{78}$$

with

$$\begin{aligned} &h_{di1}^T = \begin{bmatrix} 0 & O \end{bmatrix},\ i = 1,\ldots,v-1,\ h_{dv1}^T = \begin{bmatrix} 1 & \mathrm{m}'_{fv}(L_v) \end{bmatrix}, \\ &h_{di2}^T = \begin{bmatrix} -L_i \sin(\alpha_i - \alpha_d) - \mathrm{m}_{fi}^T(L_i) q_{fi} \cos(\alpha_i - \alpha_d) & -\mathrm{m}_{fi}^T(L_i) \sin(\alpha_i - \alpha_d) \end{bmatrix},\ i = 1,2,\ldots,v, \end{aligned} \tag{79}$$

being O a zero vector of suitable dimension.

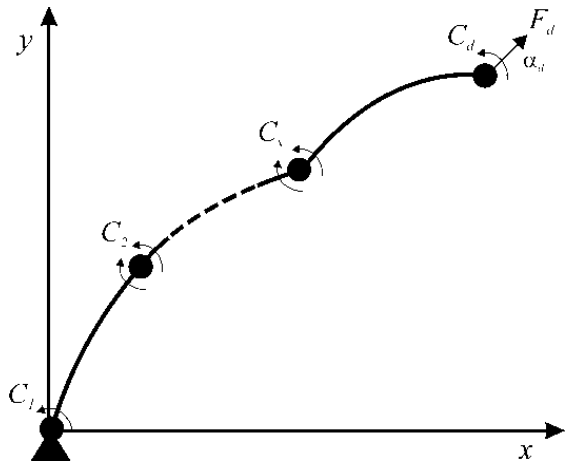

Fig. 35 Control actions and disturbances acting on the robot.

III.6 A method to reduce the computational cost

In order to reduce the computational cost of the assumed modes method, let be considered the two Lagrangian deformation variables δ and γ, which define the tip deflection and orientation of the generic flexible link.

These variables depend on the Lagrangian ones q_f as follows:

$$\begin{bmatrix} \delta \\ \gamma \end{bmatrix} = \begin{bmatrix} m_f^T(L_i) q_f \\ m_f'^T(L_i) q_f \end{bmatrix}. \tag{80}$$

Let be

$$\hat{q}_f = \begin{bmatrix} \eta_1 & \eta_2 & \cdots & \eta_{n-2} & \delta & \gamma \end{bmatrix} \tag{81}$$

the vector obtained by substituting two Lagrangian variables of the vector q_f, e.g. η_{n-1} and η_n, with the variables δ and γ.

The vectors q_f and $\hat{q}_f$ are related by the following matricial expression:

$$\begin{bmatrix} \eta_1 \\ \eta_2 \\ \vdots \\ \eta_{n-2} \\ \delta \\ \gamma \end{bmatrix} = \begin{bmatrix} 1 & 0 & \cdots & 0 & 0 & 0 \\ 0 & 1 & \cdots & 0 & 0 & 0 \\ \vdots & \vdots & \ddots & \vdots & \vdots & \vdots \\ 0 & 0 & \cdots & 1 & 0 & 0 \\ \psi_1(L) & \psi_2(L) & \cdots & \psi_{n-2}(L) & \psi_{n-1}(L) & \psi_n(L) \\ \psi_1'(L) & \psi_2'(L) & \cdots & \psi_{n-2}'(L) & \psi_{n-1}'(L) & \psi_n'(L) \end{bmatrix} \begin{bmatrix} \eta_1 \\ \eta_2 \\ \vdots \\ \eta_{n-2} \\ \eta_{n-1} \\ \eta_n \end{bmatrix}, \tag{82}$$

which can be rewritten in compact form as

$$\hat{q}_f = T q_f. \tag{83}$$

Hence, the deflection of the generic link (55) can be expressed as

$$d(z,t) = \mathrm{m}_f^T q_f = \mathrm{m}_f^T T^{-1} \hat{q}_f = \hat{\mathrm{m}}_f^T \hat{q}_f \,, \tag{84}$$

where $\hat{\mathrm{m}}_f^T$ represents the new transformed modal basis.

Remark 14. The new modal basis allows to represent the tip deflection and orientation of the generic flexible link, each of them with one Lagrangian deformation variable (δ and γ), instead of using a linear combination of all the Lagrangian deformation variables, as it has been shown in (80). The above consideration, in the light of Remark 11 and Remark 12, allows to strongly reduce the dependency of the inertia matrix and of the vector of Coriolis and centrifugal terms on the Lagrangian deformation variables; this way, significant improvements in terms of computational cost and memory usage have been obtained.

Remark 15. It is worth noting that the above linear transformation of the deformation variables does not impair the numerical stability of the model with respect to the model obtained with the classic assumed mode method.

III.7 Validation results

In this paragraph some validation results are presented, which demonstrate the computational improvement obtained with the proposed method.

Example 1. Let be considered a robot constituted by flexible links made of aluminium having square hollow constant cross-section (see Fig. 36Fig. 15) with

$L_i = 2\text{m}$, $l_i = 20\text{mm}$, $s_i = 1\text{mm}$, $E_i = 6.4 \cdot 10^{10}\,\text{N/m}^2$, $\rho_i = 2.7 \cdot 10^3\,\text{kg/m}^3$, where ρ_i denotes the density of the *i*-th flexible link.

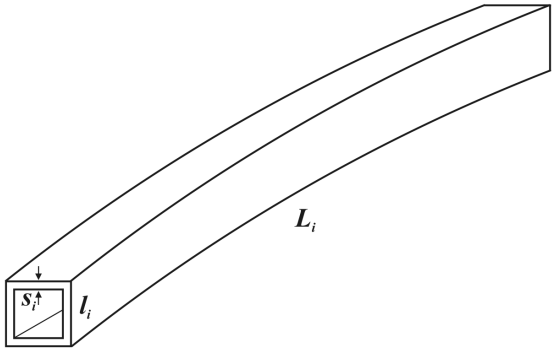

Fig. 36 *I*-th flexible link having square hollow constant cross-section.

In Table XII (Table XIII) the number of multiplications to evaluate the inertia matrix *B* (the gradient of the kinetic energy *c*) required by the classic assumed modes method and by the proposed one are compared, under the assumption that the number of modes per link is 4 and by increasing the number of links.

	optimized modal method	classic modal method	ratio
2 link	132	407	3.08
3 link	344	1178	3.42
4 link	663	2308	3.48

Table XII Number of multiplications to evaluate the inertia matrix *B* with 4 modes per link.

	optimized modal method	classic modal method	ratio
2 link	324	1052	3.24
3 link	878	2887	3.28
4 link	1705	5624	3.30

Table XIII Number of multiplications to evaluate the gradient of the kinetic energy *c* with 4 modes per link.

Note that the computational advantage of the proposed method is really notable (over 300%).

In Table XIV (Table XV) the number of multiplications to evaluate the inertia matrix B (the gradient of the kinetic energy c) required by the classic assumed modes method and by the proposed one are compared, under the assumption that the number of links is 3 and by increasing the number of modes per link.

	optimized modal method	classic modal method	ratio
3 modes	257	734	2.85
4 modes	344	1178	3.42
5 modes	448	1849	4.13

Table XIV Number of multiplications to evaluate the inertia matrix B with 3 links.

	optimized modal method	classic modal method	ratio
3 modes	665	1786	2.68
4 modes	878	2887	3.29
5 modes	1101	4391	3.99

Table XV Number of multiplications to evaluate the gradient of the kinetic energy c with 3 links.

Note that the computational advantage increases when the number of modes per link increases. The computational improvement obtained allows to reduce the time required by the dynamic simulation of the robot and to improve the implementation of the robot dynamic model in terms of memory usage.

CHAPTER IV - TRAJECTORY PLANNING

IV.1 Introduction

Trajectory planning and "kinematic" inversion for flexible robots are complex problems [27], [29], [31], both for structure flexibility and for internal and external forces, in particular the gravity one.

Moreover, the distributed parameter model of the flexible structure makes the control problem hard to solve, since the Lagrangian deformation variables used to approximate the structure flexibility are almost always not directly controllable, i.e. a joint controlled flexible structure is a sub-actuated system;

However, flexible structures must be operated and/or solicited at low frequencies, in order to avoid their breaking and/or annoying noises

Considering the above important remarks, a methodology for trajectory planning in the workspace has been developed.

IV.2 Presentation of the methodology

Let be considered a desired trajectory in the robot workspace and let it be divided into a certain number of points; for each of them a "kinematic" inversion is made, based on the static nonlinear flexible robot model, which is obtained by using the sectioning and congruence techniques known by the building science.

For each point of the trajectory, the relative joint angles are calculated which allow to rigorously obtain the desired end-effector pose; the desired joint trajectory is then obtained through suitable interpolation.

In this way the regulation problem of the end-effector is always solved. The tracking problem, instead, is solved with an error which tends to zero when the motion velocity tends to zero.

IV.3 An example of flexible static model derivation

In order to simplify the comprehension of the proposed methodology, the following example is reported in this paragraph.

Let be considered a planar flexible robot constituted by two flexible links (Fig. 37)

By using the same notations employed in Chapter I, the direct relationship which allows to express the position of the end-effector as a function of the rigid motion absolute angles results:

$$\begin{aligned} x_{o3} &= L_1 \cos\alpha_1 - \delta_1 \sin\alpha_1 + L_2 \cos\alpha_2 - \delta_2 \sin\alpha_2 \\ y_{o3} &= L_1 \sin\alpha_1 + \delta_1 \cos\alpha_1 + L_2 \sin\alpha_2 + \delta_2 \cos\alpha_2 \end{aligned} \tag{85}$$

The tip deflections δ_1 and δ_2 can be expressed as a function of the absolute angles α_1 and α_2, by using the sectioning and congruence techniques known by the building science.

In order to calculate δ_2, note that on the second link only gravitational load acts

$$q_2 = m_2 g \cos\alpha_2 ; \tag{86}$$

from (34) and from (86) it results

$$\delta_2 = -\frac{m_2 g L_2^4}{8EI}\cos\alpha_2 . \tag{87}$$

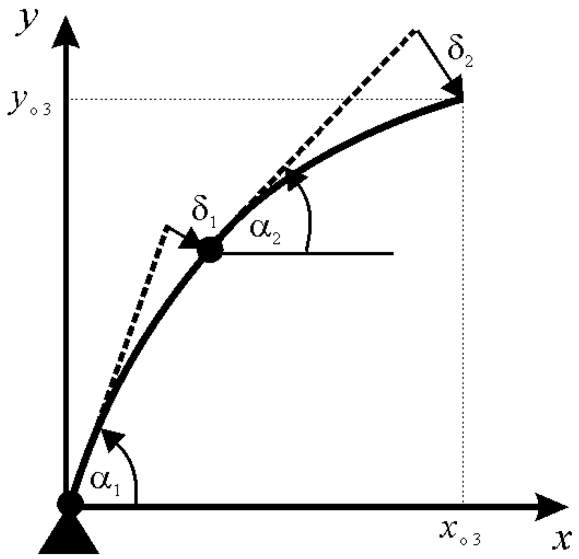

Fig. 37 Two-link flexible robot.

In order to calculate δ_1, instead, note that on the first link, in addition to the gravitational load

$$q_1 = m_1 g\cos\alpha_1 , \tag{88}$$

also a vertical force applied to the tip

$$T_{21} = -m_2 L_2 g \tag{89}$$

and a torque applied to the tip act

$$M_{21} = -\frac{m_2 g L_2^2\cos\alpha_2}{2}, \tag{90}$$

due to the effect of the second link on the first one.

The tip deflection δ_1 can be calculated by virtue of the effects superposition principle

$$\delta_1 = \delta_{1g} + \delta_{1T} + \delta_{1M} \tag{91}$$

where:

$$\delta_{1g} = -\frac{m_1 g L_1^4 \cos\alpha_1}{8EI} \tag{92}$$

is the tip deflection due to the gravity,

$$\delta_{1T} = -\frac{m_2 L_2 g \cos\alpha_1 L_1^3}{3EI} \tag{93}$$

is the tip deflection due to the vertical force T_{21},

$$\delta_{1M} = -\frac{m_2 L_2^2 g \cos\alpha_2 L_1^2}{4EI}$$

is the tip deflection due to the torque M_{21}.

By substituting the (87) and (91) into the (85) the nonlinear functions are obtained

$$\begin{aligned} x_{o3} &= f_1(\alpha_1, \alpha_2) \\ y_{o3} &= f_2(\alpha_1, \alpha_2) \end{aligned} \tag{94}$$

which can be inverted by using the powerful Matlab algorithms which solve nonlinear equations systems.

CHAPTER V - CONTROL

V.1 Calculation of an admissible nominal input

The first problem to face in the joint control of a flexible robot, when a desired joint trajectory must be followed by the motion relative angles, is the calculation of an admissible control input which should be compatible with the entire rigid-flexible robot dynamic.

At the light of the above consideration, a methodology for the dynamic inversion has been developed, which consists of the following steps:

- suitably transform the equations of the robot dynamic model so that the *n* joint control inputs appear only in *n* equations and the remaining equations result homogeneous; the above transformation is made by premultiplying both side of the differential equations system of the distributed parameter model for a transformation matrix *T*, which is obtained by placing side by side the orthogonal complement of the input matrix *H* and the input matrix *H* itself;

$$T \cdot \left(B(q)\ddot{q} + C(q,\dot{q})\dot{q} + D\dot{q} + Kq + g(q) \right) = T \cdot Hu \qquad T = \left[H^{\perp} \vdots H \right]$$

- obtain the trajectory flexible components, once the desired joint trajectory has been assigned, by solving the homogeneous equations of the transformed system;

- once all the trajectory components have been calculated, find the admissible control inputs by using the non homogeneous equations of the transformed system;

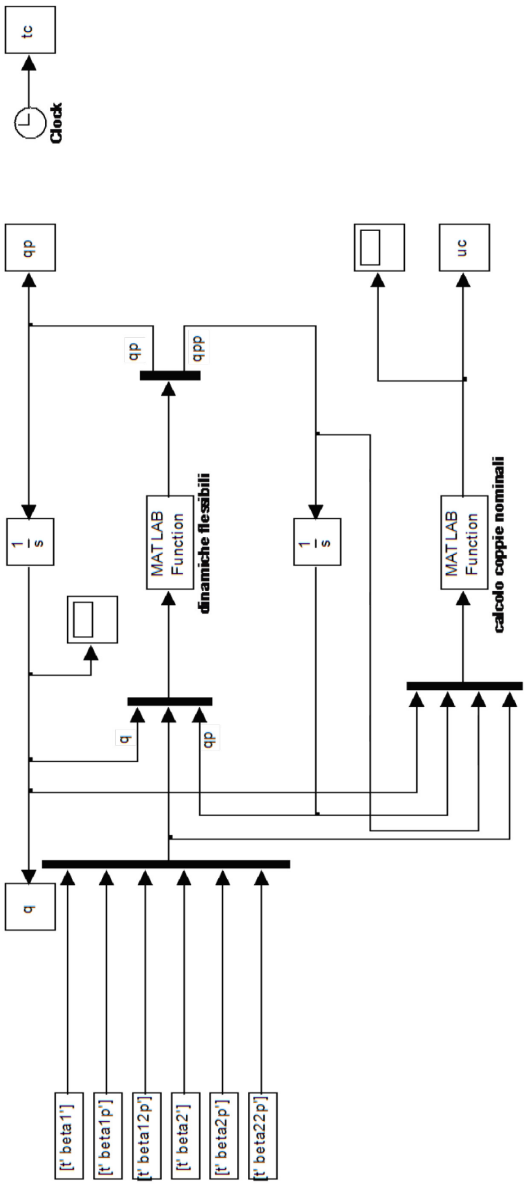

Fig. 38 Simulink block scheme for the calculation of an admissible input.

In Fig. 38 the Simulink block scheme which implements the dynamic inversion described above is reported.

In particular, it is worth noting how the transformed system of equations has been divided into a subsystem of homogeneous equations (the left Matlab function block) which is used for the calculation of the Lagrangian deformation variables dynamics, and a subsystem of non homogeneous equations, which is used for the calculation of the nominal torques (the right Matlab function block).

V.2 Controller design

The nominal nonlinear model of the flexible robot is unstable, therefore it is locally stabilized in the neighbourhood of a sufficiently high number of the trajectory points with a linear decentralized controller of PD type having the following structure:

$$h\left(a^2\left(\hat{q}_r - q_r\right) + \sqrt{2}a\left(\dot{\hat{q}}_r - \dot{q}_r\right)\right) \tag{95}$$

where

- h and a are the parameters of the controller gains;
- q_r represents the vector of the motion Lagrangian variables;
- $\hat{q}_r$ represents the vector of the motion Lagrangian variables of the nominal trajectory planned.

The stabilization is numerically obtained through the ascendant cyclic coordinates technique so to optimize the parameters $\zeta_{\min}$ (as high as possible) and $\tau_{\max}$ (as small as possible).

The global nonlinear control law is then calculated by interpolating the controller gains in the various points of the trajectory.

A controller is thus obtained, whose gains are nonlinear functions of the rigid motion coordinates and, possibly, of some measurable deformation coordinates.
The designed control law is finally validated by verifying the convergence to zero of the impulse response matrix, which is numerically calculated, and/or by using the Lyapunov theory.

V.3 A numerical example

Let be considered a planar robot constituted by two flexible links made of aluminium having square hollow constant cross section (Fig. 15) with $L_1 = L_2 = 2\text{m}$, $l_1 = l_2 = 20\text{mm}$, $s_1 = s_2 = 1\text{mm}$, $E_1 = E_2 = 6.4 \cdot 10^{10}\,\text{N/m}^2$, $\rho_1 = \rho_2 = 2.7 \cdot 10^3\,\text{kg/m}^3$

Suppose the tip must track a trajectory defined through 4 points in the work space at the time reported:

$P_1 = (-1,-1)\text{m}$ $\quad t_1 = 0\,\text{s}$
$P_2 = (-2,-1)\text{m}$ $\quad t_2 = 5\,\text{s}$
$P_3 = (-2,-2)\text{m}$ $\quad t_3 = 10\,\text{s}$
$P_4 = (-1,-2)\,\text{m}$ $\quad t_4 = 15\,\text{s}$

and suppose that the first joint of the robot is located at the origin of the work space (Fig. 37).
By using the "kinematic" inversion methodology described in Chapter IV, the relative joint angles are obtained, which guarantees, in static condition, the tip regulation (Fig. 39).

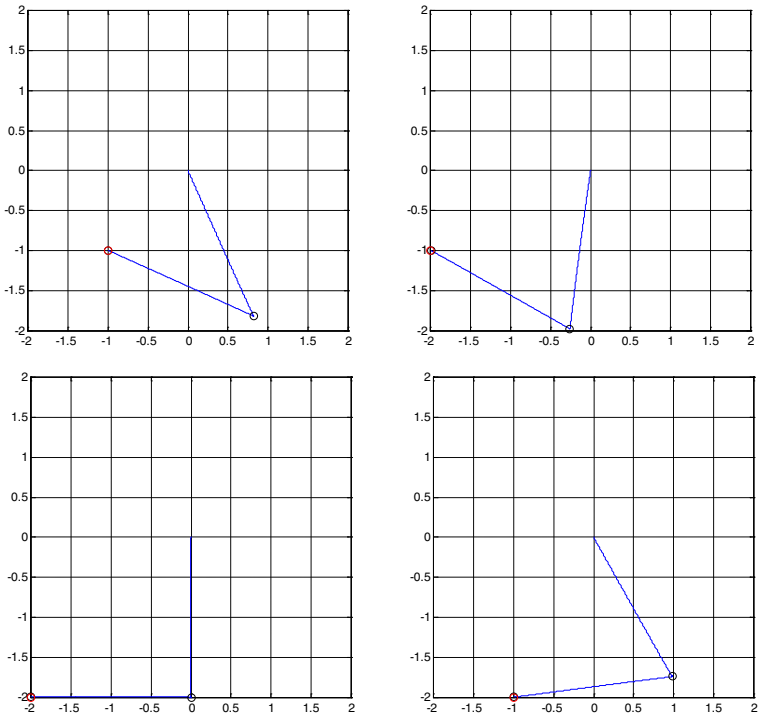

Fig. 39 Flexible robot poses in correspondence of the trajectory points.

The desired joint trajectory is thus obtained through interpolation with cubic splines (Fig. 40).

Once the above trajectory has been calculated, following the steps described in paragraph V.1, the admissible nominal (Fig. 41) input is derived.

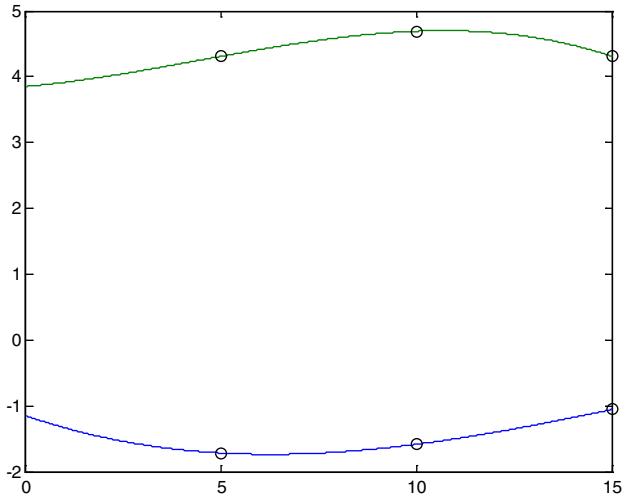

Fig. 40 The desired joint trajectory obtained through interpolation (joint 1 in blue, joint 2 in green).

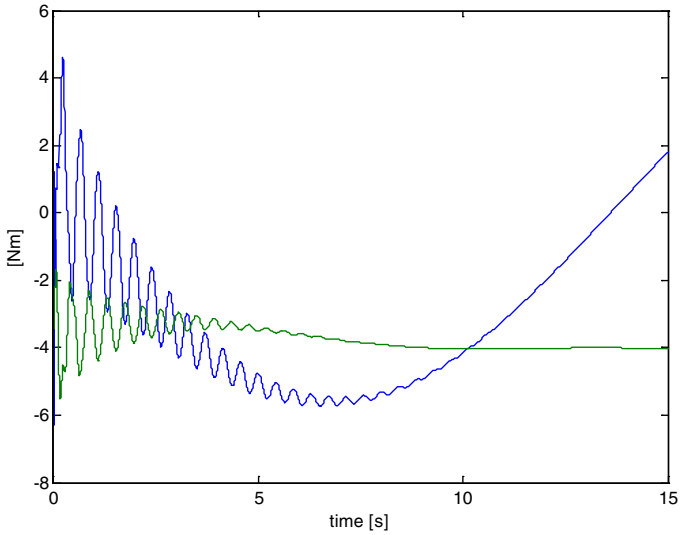

Fig. 41 Admissible nominal input.

Afterwards the system is stabilized in the neighbourhood of the trajectory points and, for each of them, the parameter h and a of the controller are obtained.

In particular, in this example, the control law has been further simplified by choosing the parameters h and a constant and equal to the max values between those calculated in the various trajectory points, i.e. $h = 25$ and $a = 5$.

The next step is to verify the linearity (in the neighbourhood of the planned trajectory) and the stability of the controlled flexible robot, by using the linear time variant systems theory. For a linear time variant system of order n, if n free responses converging to zero are found, which correspond to n independent initial conditions, the system is internally stable.

This verification has been successfully made for several values of the n initial conditions (80%, 90%, 100% of their maximum value). For example, in Fig. 42 the time diagram of the Lagrangian deformation variable δ_2 is reported.

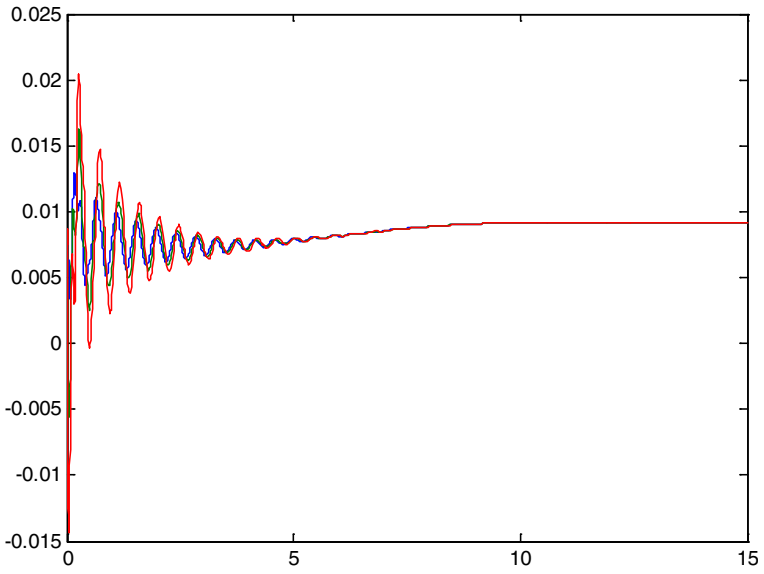

Fig. 42 Time diagram of the Lagrangian deformation variable δ_2 (100% of the initial conditions in blue, 90% of the initial conditions in green, 80% of the initial conditions in red).

Finally, in Fig. 43 the time diagram of the x and y coordinates of the tip is reported, under the assumption that the initial conditions are equal to 90% of their

nominal value. It is worth noting that the tip goes through the desired trajectory points (in red) in a satisfying manner also of the trajectory is covered with non zero velocity.

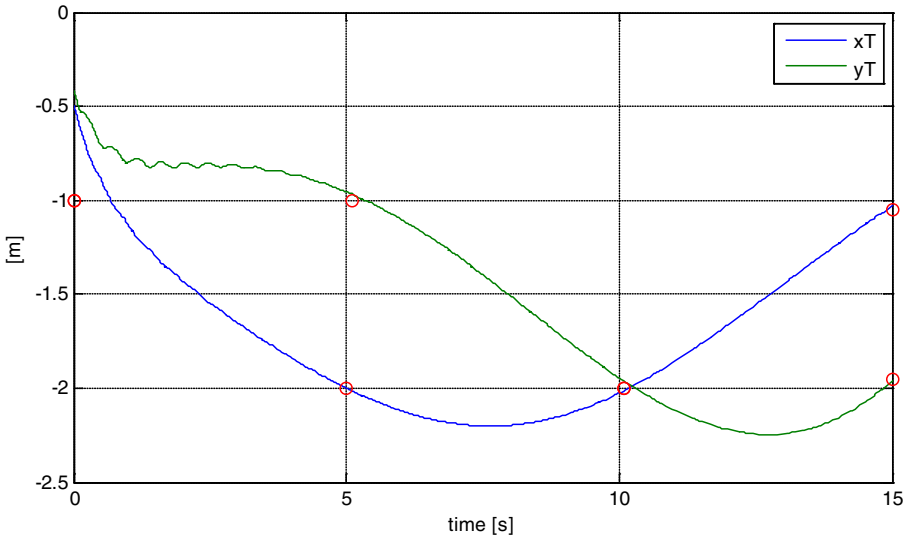

Fig. 43 Time diagram of the x and y coordinates of the tip.

BIBLIOGRAPHY

[1] S.P. Timoshenko, Strength of Materials, Part II (3rd edn), Van Nostrand, Princeton, NJ, 1956.

[2] W.J. Book, O. Maizza-Neto, and D.E. Whitney, "Feedback control of two-beam two-joint systems with distributed flexibility," ASME J. Dyn. Syst., Meas., Control, vol. 97, no. 4, pp. 424-431, 1975.

[3] W. W. Armstrong, "Recursive solution to equations of motion of an n-links manipulator," in: Proc. 5th World Congress: Theory of Machines and Mechanisms,1979, pp. 1343-1346.

[4] J. Y. S. Luh, W. M. Walker, and R. P. Paul, "On-line computational scheme for mechanical manipulators," ASME J. Dyn. Syst., Meas., Control, vol. 102, pp. 103-110, 1980.

[5] J. M. Hollerbach, "A recursive Lagrangian formulation of manipulator dynamics and a comparative study of dynamics formulation complexity," IEEE Trans. Syst., Man, Cybern., vol. 10, pp. 730-736, 1980.

[6] T. R. Kane and D. A. Levinson, "Use of Kane's dynamical equations in robotics," The Int. J. Robotics Res., vol. 2, no. 3, pp. 2-20, 1983.

[7] P. B. Usoro, R. Nadira, and S. S. Mahil, "A finite element/Lagrangian approach to modelling lightweight flexible manipulators," ASME J. Dyn. Syst., Meas., Control, vol. 108, pp. 198-205, 1986.

[8] P.C. Hughes, "Space structure vibration modes: How many exist? Which are important," IEEE Control Syst. Mag., vol. 7, pp. 22-28, 1987.

[9] G.G. Hasting and W.J. Book, "A linear dynamic model for flexible robot manipulators," IEEE Control Syst. Mag., vol. 7, pp. 61-64, 1987.

[10] P. Tomei and A. Tornambe, “Approximate modelling of robots having elastic links,” IEEE Trans. Syst., Man, Cybern., vol. 18, no. 5, pp. 831-840, 1988.

[11] B. Siciliano, and W.J. Book, “Singular perturbation approach to control of lightweight flexible manipulators.,” International Journal of Robotics Research, vol. 7, pp. 79–90, Aug 1988.

[12] C. J. Li, “A new Lagrangian formulation of dynamics for robot manipulators,” ASME J. Dyn. Syst., Meas., Control, vol. 11, pp. 559-567, 1989.

[13] A.J. Calise, J.V.R. Prasad, and B. Siciliano, “Design of optimal output feedback compensators in two-time scale systems,” IEEE Transactions on Automatic Control, vol. 35, pp. 488–492, Apr 1990.

[14] A. De Luca and B. Siciliano, “Closed form dynamical model of planar multilink lightweight robots,” IEEE Trans. Syst., Man, Cybern., vol. 21, no. 4, pp. 826-839, 1991.

[15] Kao, C. K. and Sinha, A., “Sliding mode control of vibration in flexible structures using estimated states,” Proceedings of the American Control Conference, vol. 3, pp. 2467–2474, 1991.

[16] D. Wang and M. Vidyasagar, “Modelling a class of multilink manipulators with the last link flexible,” IEEE Trans. Robot. Autom., vol. 8, no. 1, pp. 33-41, 1992.

[17] C. J. Li and T. S. Sankar, “Systematic methods for efficient modelling and dynamics computation of flexible robot manipulators,” IEEE Trans. Syst., Man, Cybern., vol. 23, no. 1, 1993.

[18] Z.H. Luo, “Direct strain feedback control of flexible robot arms: new theoretical and experimental results,” IEEE Transactions on Automatic Control, vol. 38, no. 11, pp. 1610–1622, 1993.

[19] W. Yu, “Mathematical modelling for a class of flexible robot,” Appl. Math. Model., vol. 19, no. 9, pp. 537-542, 1995.

[20] S. Nicosia, P. Valigi, and L. Zaccarian, “Dynamic modelling of a two link flexible robot and experimental validation,” in: Proc. 1996 IEEE Int. Conf. on Robot. and Autom., Minneapolis, Minnesota, Apr. 1996, pp. 1953-1958.

[21] G. Ambrosino, G. Celentano, and R. Setola, “Integrated model of a flexible beam with piezoelectric plates for active vibration control,” in: Proc. 13th IFAC World Congress, San Francisco, USA, 1996, pp. 261-266.

[22] P. Rocco, and W.J. Book, “Modelling for two-time scale force/position control of flexible robots,” in Proceedings. 1996 IEEE International Conference on Robotics and Automation, vol. 3, pp. 1941–1946, 1996.

[23] M.O. Tokhi, Z. Mohamed, and A.K.M. Azad, “Finite difference and finite element approaches to dynamic modelling of a flexible manipulator,” in: Proc. Inst. Mech. Eng. I, J. Syst. Control Eng., vol. 211, no. 2, 1997, pp. 145-156.

[24] G. Celentano and R. Setola, “The modelling of a flexible beam with piezoelectric plates for active vibration control,” J. Sound Vibrat., vol. 223, no. 3, pp. 483-492, 1999.

[25] F. Boyer and W. Khalil, “Kinematic model of a multi-beam structure undergoing large elastic displacement and rotations. Part one: model of an isolated beam,” J. Mech. Mach. Theory, vol. 34, pp. 205-222, 1999.

[26] Xu, J. X. and Cao, W. J., “Active vibration control of a single-link flexible manipulator by pole-placement approach,” Proceedings of the 38th IEEE Conference on Decision and Control, vol. 4, pp. 3888–3893, 1999.

[27] B. Siciliano, “Closed-loop inverse kinematics algorithm for constrained flexible manipulators under gravity,” J. Robot. Syst., vol. 16, no. 6, pp. 353-362, 1999.

[28] I. Narayan Kar, K. Seto, and F. Doi, "Multimode vibration control of a flexible structure using H_∞-based robust control," IEEE/ASME Trans. Mechatronics, vol. 5, no. 1, pp. 23-31, Mar. 2000.

[29] H. Yang, H. Krishnan and M.H. Ang, Jr., "Tip-trajectory Tracking Control of Single-Link Flexible Robots by Output Re-definition," Control Theory and Applications, IEE Proceedings, vol. 147, no. 6, pp. 580-587, 2000.

[30] Hisseine, D. and Lohmann, B., "Robust control for a flexible-link manipulator using sliding mode techniques and nonlinear H_∞ control design methods," Proceedings – IEEE International Conference on Robotics and Automation, vol. 4, pp. 3865–3870, 2001.

[31] B. Siciliano and L. Villani, "An inverse kinematics algorithm for interaction control of a flexible arm with a compliant surface," Control Eng. Practice, vol. 9, pp. 191-198, 2001.

[32] R.D. Robinett, C. Dohrmann, G.R. Eisler, J. Feddema, G.G. Parker, D.G. Wilson, and D. Stokes, Flexible Robot Dynamics and Controls, Kluver Academic/Plenum Publishers, New York, 2002.

[33] A.J. Calise, B.J. Yang, and J.I. Craig, "An augmenting adaptive approach to control of flexible systems," in Proceedings of AIAA Guidance, Navigation, and Control Conference, vol. AIAA-2002-4942, 2002.

[34] Yang, B.-J., Calise, A. J., and Craig, J. I., "Adaptive output feedback control with input saturation," in Proceeding of the American Control Conference, vol. 2, pp. 1572–1577, June 2003.

[35] Yang, B.-J., Adaptive Output Feedback Control of Flexible Systems. PhD thesis, Georgia Institute of Technology, School of Mechanical Engineering, Apr. 2004.

[36] T.H. Megson, Structural and stress analysis, Butterworth-Heinemann, Oxford, 2005.

[37] C. La-orpacharapan and L.Y. Pao, “Fast and robust control of systems with multiple flexible modes,” IEEE/ASME Trans. Mechatronics, vol. 10, no. 5, pp. 521-534, Oct. 2005.

[38] S.C.P Gomes, V.S. da Rosa, and Bd.C. Albertini, “Active control to flexible manipulators,” IEEE/ASME Trans. Mechatronics, vol. 11, no. 1, pp. 75-83, Feb. 2006.

[39] L. Celentano, “Modellistica e Controllo dei Sistemi Meccanici Rigidi e Flessibili,” PhD Thesis, Dipartimento. di Informatica e Sistemistica, Università degli Studi di Napoli Federico II, Napoli, Italy, Nov. 2006. Available: www.fedoa.unina.it/view/people/Celentano,_Laura.html.

[40] L. Celentano and R. Iervolino, “New results on robot modelling and simulation,” ASME J. Dyn. Syst., Meas., Control, vol.128, pp. 811-819, 2006.

[41] Krauss, R. W. An Improved Technique for Modeling and Control of Flexible Structures, Georgia Institute of Technology, School of Mechanical Engineering, Apr. 2006.

[42] A. Macchelli, C. Melchiorri, and S. Stramigioli, “Port-based modelling of a flexible link,” IEEE Trans. Robot., vol. 23, no. 4, pp. 650-660, 2007.

[43] L. Celentano, New Approaches in Automation and Robotics, Harald Aschemann (Ed.), I-Tech Education and Publishing, Vienna, Austria, May 2008, ch. 10, pp. 173-196.

[44] B. Siciliano and O. Khatib, Springer Handbook of Robotics, Springer, 2008.

[45] I.A. Mahmood, S.O.R. Moheimani, and B. Bhikkaji, “Precise tip positioning of a flexible manipulator using resonant control,” IEEE/ASME Trans. Mechatronics, vol. 13, no. 2, pp. 180-186, Apr. 2008.

[46] L. Celentano and A. Coppola, “An innovative method to modeling flexible robots”, submitted to Applied Mathematical Modeling, Nov. 2009.

[47] L.Celentano, A. Coppola, "A Computation Efficient Method to Modeling Flexible Robots with the Assumed Modes Method“, submitted to Applied Mathematics and Computation, Jun 2010.

[48] L. Celentano and A. Coppola, “A Wavelet Based Method to Modeling Realistic Flexible Robots”, submitted to IFAC 2011, Sep. 2010